CONTRACT REPORT S-68-1

INVESTIGATION OF GROUND SHOCK EFFECTS IN NONLINEAR HYSTERETIC MEDIA

Report 1

DEVELOPMENT OF MATHEMATICAL MATERIAL MODELS

by

Ivan Nelson
Melvin L. Baron

March 1968

Sponsored by

Defense Atomic Support Agency

Conducted for

U.S. Army Engineer Waterways Experiment Station
CORPS OF ENGINEERS
Vicksburg, Mississippi

Under

Contract No. DACA39-67-C-0048

by

Paul Weidlinger, Consulting Engineer
New York, New York

CONTRACT REPORT S-68-1

INVESTIGATION OF GROUND SHOCK EFFECTS IN NONLINEAR HYSTERETIC MEDIA

Report 1

DEVELOPMENT OF MATHEMATICAL MATERIAL MODELS

by

Ivan Nelson
Melvin L. Baron

March 1968

Sponsored by

Defense Atomic Support Agency

Conducted for

U.S. Army Engineer Waterways Experiment Station
CORPS OF ENGINEERS
Vicksburg, Mississippi

Under

Contract No. DACA39-67-C-0048

by

Paul Weidlinger, Consulting Engineer
New York, New York

FOREWORD

The initial investigations of plastic models described in this report were carried out under Contract No. DA-49-146-XZ-508 for the Defense Atomic Support Agency (DASA). The current work on variable moduli models is part of Contract No. DACA 39-67-C-0048, "Investigation of Ground Shock Effects in Nonlinear Hysteretic Media," being conducted for the U. S. Army Engineer Waterways Experiment Station (WES) under DASA sponsorship.

This work has been done in close cooperation with the WES Project Engineer, Mr. J. G. Jackson, Jr. The authors wish to thank him for his assistance in describing the behavior of real materials. They also wish to acknowledge the contribution of Dr. Hans H. Bleich, Consultant, to the early theoretical development of the plastic and the variable moduli models.

The WES contract is under the general supervision of Mr. W. J. Turnbull, Chief, Soils Division. COL Levi A. Brown, CE, is the Contracting Officer.

ABSTRACT

A historical outline of mathematical models used previously to represent soil and rock behavior in ground shock computations at low pressure levels is presented. The problems and deficiencies of these early approaches are discussed. Subsequently, two types of models are developed; one a plastic model in which the yield condition depends on the mean stress and in which different variable bulk moduli are used in loading and unloading. The second type of model, called the "variable moduli model", has variable shear as well as bulk moduli, but no explicit yield condition. The behavior of both types of model in uniaxial strain and triaxial compression tests is examined.

DEVELOPMENT OF MATHEMATICAL MATERIAL MODELS

Table of Contents

LIST OF SYMBOLS

A_1 , A_2	Area in stress-strain curve, Fig. (2).
c	Constant in yield condition, see Eqs. (I-5), (I-9).
c_1 , c_2 , c_3	Constants.
E	Young's modulus.
e	Mean strain.
e_o	Initial mean strain in triaxial test.
e_{ij}	Components of deviatoric strain tensor.
e_1 , e_2 , e_3	Principal deviatoric strains.
G	Shear modulus.
G_o , G_1 , $\bar{G}_1$	Constants in shear modulus.
G_{UN}	Shear modulus in unloading.
h	Step function.
I_2'	Second invariant of strain deviator.
J_1	First invariant of stress tensor.
J_2'	Second invariant of stress deviator.
$J_{1,LIQ}$	Constant appearing in K_{UN} in alluvium-playa model.
K	Bulk modulus.
K_o , K_1 , K_2	Constants appearing in bulk modulus.
K_{LD} , K_{UN}	Bulk modulus in loading - unloading.
k	Constant related to cohesion.
M	Constrained modulus.
p	Pressure.
s_{ij}	Components of deviatoric stress tensor.
s_1 , s_2 , s_3	Principal deviatoric stresses.

α	Coefficient of J_1 in Coulomb yield condition.
$\bar{\alpha}$	Variable α.
β	Constant, $2(1+\nu)/(1-2\nu)$.
γ	Constant in alluvium-playa bulk relation.
γ_1 , $\bar{\gamma}_1$	Constants in combined variable shear modulus.
δ_{ij}	Kronecker delta.
Δe_{ij}	Change in deviatoric strain in time step.
$\Delta\varepsilon_1$	Measured axial strain in triaxial test.
ε_{ij}	Components of strain tensor.
ε_1 , ε_2 , ε_3	Principal strains.
ε_{kk}	Volumetric strain, 3e.
η, $\bar{\eta}$	Constants appearing in Fig. (2).
ν	Poisson's ratio.
ν_o	Poisson's ratio at zero stress and strain.
ξ	Variable of integration.
ρ	Density.
ρ_o	Initial density.
σ_{ij}	Components of stress tensor.
σ_1 , σ_2 , σ_3	Principal stresses.
ϕ	Angle of internal friction of granular material.

I INTRODUCTION.

The growing interest in the determination of the response of structures at relatively high pressure contours has stimulated the study of ground shock from both direct and air induced sources. As the investigations have progressed into the range of thousands of psi air overpressure contours, the studies of combined air and direct ground shock, as well as air-induced ground shock only have required the development of considerably more complicated and, hopefully, more accurate material models. Whereas previously, air-induced ground shock effects at low overpressure levels were approximated by means of linearly elastic models, the requirements of problems involving combined air and direct ground shock effects necessitated a definition of the material behavior in a range extending from the hydrodynamic behavior at extremely high pressure regions in the neighborhood of Ground Zero, through various types of inelastic solid material regions and finally to essentially elastic ranges at sufficiently low pressures. Parallel to the theoretical development of these more realistic material models have been the difficult demands on the experimentalists for tests which would mirror the behavior of the material throughout the entire range of pressures. The tests served two major purposes: (a) to give an idea of the proper type of material behavior as an aid in the mathematical modeling of the soil or rock at appropriate pressure levels, and (b) to provide data from which the required material constants in the mathematical models could be determined.

In the high pressure range (say above 100 KB) Hugoniot data is obtained from high velocity impact flying plate tests. In the lower range from about 5 KB to 80 KB, data is presently being obtained from both flying plate tests and explosive tests with spherically diffusing wave geometries. Below 2 KB, the usual soil tests of uniaxial strain and triaxial compression are utilized. Unsupported uniaxial compression tests which are run for rock are essentially a special case of a triaxial compression test in which the lateral stress σ_3 is zero.

For a given soil, the uniaxial strain and triaxial compression tests give the most detailed information and are generally utilized in the development of the mathematical model, particularly in those cases in which air-induced ground shock only is being studied. Typical experimental curves for each test are shown in Fig. (1). The stress-strain curve in the uniaxial strain case, Fig. (1a), typically shows a reversal in curvature on loading. On unloading, the slope is almost constant and is much larger than the slope during initial loading, except for a sharp tail in the low stress range. Reloading generally follows the unloading curve up to the previous maximum stress and then continues along the initial loading curve. The lateral stress σ_3, required to maintain uniaxial strain, is sometimes also measured, Fig. (1b).

In the triaxial compression tests, the stress-strain curves, Fig. (1c), are concave downward up to a horizontal

tangent at what is called "failure". Different curves are obtained for different values of the confining stress σ_3 . Although the lateral strain ε_3 is not generally available, experimental work, currently in progress, is aimed at providing this information. By plotting the Mohr's circles at failure for different lateral stresses σ_3 , the Mohr envelope, Fig. (1d), is obtained. This envelope is generally either a straight line (for some dry sands) or is concave downward (for partially saturated soils). Both the theoretical and the experimental programs have made considerable progress in recent years. The present paper will describe some of the recent theoretical approaches which have been and are being used in the development of the material models.

Before discussing these models, it is perhaps of some interest to review the development of material models from a historical viewpoint. Originally, linearly elastic models were used in the analysis of air-induced ground shock effects at low pressure levels (20-100 psi contours). As technological changes in weapons design and delivery systems forced the locations of the hardened structures to considerably higher overpressure levels, inelastic effects were introduced into the analysis. For the most part, these effects consisted of introducing a yield condition into the material model of the form suggested by Prager and Drucker, Ref. [1]:

$$\alpha J_1 + \sqrt{J_2'} = k \qquad \text{(I-1)}$$

or a condition of the von Mises type

$$\sqrt{J_2'} = k \tag{I-2}$$

where α is a coefficient which depends upon the angle of internal friction of the material, k is a constant proportioned to the cohesion, $J_1 = -3p$ is the first invariant of the stress tensor, and J_2' is the second invariant of the stress deviators. The early models of materials which were assumed to act linearly elastic below certain stress configurations and to obey the yield condition of Eq. (I-1) were called Coulomb materials with cohesion or Prager-Drucker materials.

A considerable amount of both numerical and theoretical work has been done for the special case in which the cohesion constant k was taken to be zero, Refs. [2], [3], [4], and [5]. Such materials have been called Coulomb materials and satisfy the yield condition

$$\alpha J_1 + \sqrt{J_2'} = 0 \tag{I-3}$$

For cases in which the yield condition satisfies Eq.(I-1) or Eq.(I-3), the materials have a conical yield surface and exhibit the phenomenon of dilation, that is, an inelastic volume increase when loaded to sufficiently high stress in compression and subsequently unloaded. Figure (2) shows typical stress-strain plots for such materials in a uniaxial strain compression test configuration. It is seen that upon full unloading, a net residual extension is obtained for this

essentially one-dimensional configuration. In three-dimensional problems (two dimensional space-time), this manifests itself in an inelastic increase of the volume. The von Mises material, on the other hand, which satisfies the yield condition of Eq. (I-2), has a cylindrical yield surface and exhibits no dilatancy effects as shown in Fig. (2). Theoretical solutions to several problems have also been obtained for the von Mises material, Refs. [6], [7], and [8]. Problems arose in the use of both of these models. First and perhaps foremost was the dilatancy effect from the dependence of $\sqrt{J_2'}$ on J_1 in the yield condition for the Coulomb material model. While such phenomena have been observed in certain types of sands under special loading conditions, this is certainly not typical of many of the soils and rocks which are encountered in practical design problems. The von Mises material on the other hand, requires that the material maintain essentially the same shear strength at all stress levels, since no variation in $\sqrt{J_2'}$ is allowed in the yield condition as the stress range increases and hence, $|J_1|$ increases. While such a situation is probably quite true at extremely high pressure levels, e.g., as the material passes from a hydrodynamic to a solid state, it is certainly not generally true at lower stress levels in which tests usually show that an increase in $\sqrt{J_2'}$ before yielding occurs as J_1 increases. Consequently, two problems arose: (1) while many materials of interest acted essentially as a Coulomb material at low pressures, at higher pressures they

acted as a von Mises material and consequently, the mathematical material model would have to act in a similar fashion, and (2) the Coulomb model would have to be amended so that it had a zero net dilation at the end of a complete loading-unloading cycle*).

The next advance in model development was the introduction of a nonlinear pressure-volume relation, i.e., a variable bulk modulus $K = K(J_1)$, in the material description. At the same time, the shear modulus G was kept constant**). The use of the variable bulk modulus, in addition to giving the proper concavity to the stress-strain curve from a uniaxial compression test, aided materially in obtaining a smooth transition at high pressures from the hydrodynamic material (governed by a suitable equation of state) to the solid inelastic material. In the neighborhood of the transition, the solid inelastic material acts as a von Mises material with a nonlinear pressure-volume relation. By properly choosing the

---

*) In any material in which the plastic flow rule is derivable from a yield condition which depends on the mean pressure p (or the first invariant J_1), the incremental dilation cannot be zero but the net dilation from a complete loading-unloading cycle may be eliminated.

**) A model in which the shear modulus G was made a function of J_1 in unloading was also considered, but extensive numerical ground shock calculations were not made for this model.

constants in the expression $K = K(J_1)$, the shock velocities for the inelastic solid material in the selected transition range may be matched to those given by the equation of state of the hydrodynamic material in this range, thus eliminating possible impedance mismatches and resulting in a smooth transition.

The problem of modeling a material which obeyed a Coulomb type yield condition at low pressures and a von Mises yield condition at higher pressures was solved by requiring a smooth transition between the two conditions through the use of a yield condition of the form

$$f(J_1) + \sqrt{J_2'} = k \tag{I-4}$$

where the function of J_1 was chosen so that the material had the proper behavior in the appropriate ranges, e.g., essentially Coulomb at low values of the mean pressure p and von Mises at high values. In an early version of this type of model for a volcanic tuff, the relation

$$\alpha\left(1 + \frac{J_1}{c}\right)^2 J_1 + \sqrt{J_2'} = k \qquad |J_1| < c \tag{I-5}$$

$$\sqrt{J_2'} = k \qquad |J_1| \geq c \tag{I-6}$$

was utilized, Fig. (3), together with the relations

$$K = K_o - K_1 J_1 + K_2 J_1^2 \tag{I-7}$$

$$G = G_o \tag{I-8}$$

In this model the constants K_o, G_o, α, and k were chosen from whatever information was available from triaxial compression (α and k) and uniaxial strain (K_o and G_o) tests. The constants K_1 and K_2 were chosen to make the shock velocities from the hydrodynamic equation of state model (which was used in the higher pressure ranges) match those from the solid inelastic material model over a 20 KB to 100 KB range of mean pressures. From Fig. (3) it is seen that the yield condition in this model was chosen such that a smooth transition exists between the Coulomb type material and the von Mises type material. Since the cohesion constant k was kept the same at both low and high values of J_1, a reversal in curvature, as shown, was obtained for the yield surface. This model was inherently questionable because of this negative curvature of the yield surface, since uniqueness has not been mathematically proved for such cases. It represented one of the very early models of this type and has long been superseded by what we consider to be more accurate models which are described in detail later in this report.

The later models utilized a yield condition of the form

$$\sqrt{J_2'} = k - \alpha J_1\left(1 + \frac{J_1}{2c}\right) \qquad J_1 + c > 0 \qquad \text{(I-9)}$$

$$= k + \frac{\alpha c}{2} \qquad J_1 + c < 0 \qquad \text{(I-10)}$$

as shown in Fig. (4). Again, the condition approximates the Coulomb material at low pressures and a von Mises material

at high pressures, while the transition surface is such that the curvature is positive over the entire surface, a sufficient condition for uniqueness. A detailed discussion of a model in which the yield condition is utilized is given in Section II for an alluvium-playa material.

The use of different nonlinear pressure-volume relations, i.e., nonlinear bulk moduli in loading and unloading enables one to eliminate the net dilation for a complete loading-unloading cycle in uniaxial strain, Fig. (5). This also satisfies the requirement of a steep unloading slope as found in the experiments.

It is in order to make some general observations regarding the problems involving dilation, particularly those which arise in reloading situations. In material models which utilize plastic yield conditions, it is usually advisable to derive the flow rule from a plastic potential which is identical to the yield condition, since for such cases, uniqueness theorems have been derived for specific yield conditions such as the von Mises and Coulomb conditions, and can be deduced for other more generalized cases. The introduction into the model of a nonlinear pressure - volume relation together with the yield condition creates no new difficulties when the same curve is used for both loading and unloading. While this may be permissible in some ranges for certain types of rocklike materials, there are many other rock and soil materials for which, in the range of interest, material property tests indicate important hysteretic energy losses in a complete loading-unloading cycle.

In mathematical models for such materials, different K and G relations must be used in loading and unloading. This may lead, however, to problems on reloading as shown in Fig. (6). For example, if we load, unload, and then reload along the unloading curve until the original loading curve is reached, we will generally find ourselves off the original loading curve because of the inherent dilatancy effect (inelastic volume change) in the material if a yield condition is used in which the first invariant J_1 of the stress tensor appears. The question of how to return to the original loading curve arises and is not an easily answered one. For example, one way of doing this would be to use a yield condition of the form $f(J_1) + \sqrt{J_2'} = k$, but at the same time use a flow rule derivable from a plastic potential of the type $F = \sqrt{J_2'} - k$. Such a procedure would still determine yielding by the general yield condition, but would correct for the yielding by changing only the stress deviators, and no change would be made in the mean pressure $p = -\frac{J_1}{3}$ in the correction for yielding. This procedure would eliminate any incremental dilation effect in any portion (time step) of the numerical calculations. This approach has been used in several of the existing codes. Another possibility might be to return to the original P-V curve by some sort of interpolation procedure. A third possibility would be to continue loading along a curve parallel to the original P-V curve. There are several possibilities no one of which can be said to be correct as compared to the physical evidence for real materials.

It is important, however, to determine the sensitivity of the various models to the several possible procedures. Investigations of these effects are currently being made.

An alternative approach to the determination of mathematical models has led to a series of what we call "variable moduli" models. In these cases, the bulk modulus K and the shear modulus G are assumed to be functions of appropriate stress and/or strain tensor invariants, and no plastic yield conditions are specified for the material. Different functional relationships for K and G are used in loading and unloading. The study of such models is relatively recent and has been confined at this time to theoretical investigations. It is hoped that the work will be applied to the analysis of real materials in ground shock problems in the near future.

The models are developed by requiring that the truncated series expansions for both K and G in terms of stress and/or strain tensor invariants have their constants chosen so that the three-dimensional model conforms to both the triaxial compression and the uniaxial strain results when it is run for these configurations. Once the appropriate form of the K and G functions is determined, the constants appearing in these expressions are determined by means of a curve-fitting routine from uniaxial strain and triaxial compression test data for a given soil.

One possible advantage of these models is that they accurately reproduce the available test data from the material property tests that are generally made. This is an advantage over the previously discussed plastic models in which K was a function of J_1 and G was kept constant. In the latter case, excellent reproductions of uniaxial strain results were obtained, but the results from triaxial compression tests were not reproduced. The combination of the two types of models, namely a variable modulus model which also satisfies a yield condition, has not yet been studied in detail.

Section III describes three of the variable moduli models that have been studied thus far. Conclusions are presented regarding their suitability as models for real soil materials. While the studies on the variable moduli models are still at a relatively early stage, it appears that this approach shows promise.

II NONLINEAR PLASTIC MATERIAL MODEL - ALLUVIUM-PLAYA.

The model utilizes a nonlinear bulk modulus and a constant shear modulus, together with a modified Prager-Drucker yield condition. The yield condition is of the form

$$\sqrt{J_2'} = k - \alpha J_1 \left(1 + \frac{J_1}{2c}\right) = k - \bar{\alpha}(J_1)J_1 \qquad J_1 + c > 0 \qquad \text{(II-1)}$$

$$= k + \frac{\alpha c}{2} = k_{\text{effective}} . \qquad J_1 + c < 0 \qquad \text{(II-2)}$$

This condition approximates the Prager-Drucker condition for $|J_1| << c$, while in the high pressure range, the material behaves as a von Mises material with $k = k_{\text{effective}}$, Fig. (4). At $J_1 = -c$, a smooth transition occurs. It is of interest to note that in this model, the value of the cohesion constant k at low pressures is less than the corresponding constant $k_{\text{effective}} = k + \frac{\alpha c}{2}$ at higher pressures, thus resulting in a transition yield surface which maintains a positive curvature, a sufficient condition for uniqueness.

From available test information, in particular uniaxial strain test data, it was noted that this material exhibited a considerable amount of hysteresis in a loading-unloading cycle. In order to obtain the proper amount of hysteresis in the mathematical model, different pressure-volume relations were used for loading and unloading. These relations were defined by variable bulk moduli through the relation

$$\dot{J}_1 = 3K(J_1)\ \dot{\varepsilon}_{kk} \qquad \text{(II-3)}$$

The shear modulus $G = G_o$ was kept constant for initial loading.

In uniaxial strain, experimental information showed that this material is characterized by an initial softening and a subsequent hardening, Fig. (1a). The simple quadratic relation for the bulk modulus, Eq. (I-7), used previously in the earlier tuff model, was not sufficient to both match the hydrodynamic material shock velocities at high pressures and to provide the proper curvature for the stress-strain curve at lower pressures. Consequently, an altered bulk modulus was used for higher pressures $|J_1| > \gamma c$. At lower pressures, $|J_1| < \gamma c$, the simplest expression which yields an initial negative curvature in ur'axial strain and which matches the value of the higher pressure K relation at $|J_1| = \gamma c$ was used. The initial loading bulk modulus K is given by the relation

$$K_{LD}(J_1) = [K_o - \frac{\gamma c}{4} K_1] + \frac{K_1}{\gamma c} [J_1 + \frac{\gamma c}{2}]^2 \qquad |J_1| < \gamma c \quad \text{(II-4)}$$

$$= K_o - K_1(J_1 + \gamma c) + K_2(J_1 + \gamma c)^2 \qquad |J_1| > \gamma c \quad \text{(II-5)}$$

so that $K_{LD} = K_o$ = elastic bulk modulus when $J_1 = 0$ and again when $J_1 = -\gamma c$. Between these values of J_1, K_{LD} drops to a minimum at $J_1 = -\frac{\gamma c}{2}$. At $J_1 = -\gamma c$, both K_{LD} and its derivative with respect to J_1, i.e., $\frac{dK_{LD}}{dJ_1}$, are continuous. Above $J_1 = -\gamma c$, K_{LD} increases monotonically.

At very large pressures, one might expect the material to behave essentially as a fluid (little or no energy dissipation) with similar loading and unloading characteristics. A quantity $J_{1,LIQ}$ is defined as a measure of the pressure above which the behavior of the material in loading and unloading is similar. Below $J_{1,LIQ}$, particularly where experimental data is available, it appears that the slope of the unloading curve in uniaxial strain is considerably greater than the corresponding loading curve slope, thus indicating a considerable amount of energy dissipation in this material. Moreover, the unloading slope appears to diminish gradually. The bulk modulus for unloading was chosen to give this behavior, and is given by

$$K_{UN}(J_1) = K_o - K_1 J_1 + K_2 J_1^2 \qquad J_1 + J_{1,LIQ} < 0 \qquad \text{(II-6)}$$

$$= K_4 \sqrt{1 - \frac{\alpha}{k} J_1} \qquad J_1 + J_{1,LIQ} > 0 \qquad \text{(II-7)}$$

where

$$K_4 = \frac{K_o + J_{1,LIQ} K_1 + J_{1,LIQ}^2 K_2}{\sqrt{1 + \frac{\alpha J_{1,LIQ}}{k}}} \qquad \text{(II-8)}$$

is chosen so that K_{UN} is continuous at $J_1 = -J_{1,LIQ}$. Note that the quantity $\frac{dK_{UN}}{dJ_1}$ is discontinuous at this point. The value of K_{UN} can never be zero since $J_1 < \frac{k}{\alpha}$ by the yield condition requirements. When $|J_1| > J_{1,LIQ} >> Yc$, K_{UN} is always greater than K_{LD}, but the difference is small.

Below $J_1 = -J_{1,LIQ}$, K_{UN} very gradually decreases with decreasing pressure until at very low pressure K_{UN} decreases rapidly. Figure (7) shows a typical diagram of the relation between K and J_1 for both loading and unloading.

With respect to the shear modulus G in unloading, three different variations of the model have been considered. First, the same constant G_o was used in both loading and unloading for a series of ground shock calculations for an alluvium-playa medium. Secondly, a constant value of $G = G_{UN}$ which differs from the initial loading shear modulus G_o was studied theoretically. Finally, a variation in which the shear modulus on unloading has been allowed to vary as a function of $K_{UN}(J_1)$ over a portion of the region,

$$G = G_o \quad \text{when } s_{ij} \Delta e_{ij} > 0 \tag{II-9}$$

$$G = \frac{G_o}{2}\left[1 + \frac{K_{UN}(J_1)}{K_o}\right] \quad \text{when } s_{ij} \Delta e_{ij} < 0 \tag{II-10}$$

has been studied theoretically.

The determination of the various constants which appear in the model was based predominantly on uniaxial strain test data. Attempts to make the model also fit available information on the Mohr failure envelope from triaxial compression tests were unsuccessful. Since the geometry for the ground shock problems are closer to a uniaxial strain test configuration than to that of a triaxial compression test, the model was chosen to conform as closely as possible to the uniaxial strain experimental data. The constants K_o and G_o were chosen from the uniaxial strain data, while the

constants K_1 and K_2 were determined so that in the higher pressure ranges (say 20 KB - 90 KB) the shock velocities of the solid material matched those from the hydrodynamic equation of state material over this range of pressures. The constant γ was chosen so that the strain at the point of inflection of the uniaxial stress-strain curve falls within the range of the experimental values. The quantity c was determined from available strength data while the constant $J_{1,LIQ}$ was essentially guessed. As new experimental results into higher pressure ranges become available under the present DASA experimental program, it is hoped that the $J_{1,LIQ}$ value may be determined directly from the test data. The plastic constants α and k were approximately determined from triaxial compression data and were modified to make the model conform to the uniaxial strain results.

Theoretical curves for the uniaxial strain test are presented in Figs. (8)-(9) for the plastic model described in this section. The results are for the case in which G_{UN} is given by Eqs. (II-9) - (II-10). The following constants were used in the calculations

G_o = 0.5 KB	α = 0.15	ρ_o = 1.6 gm/cm^3
K_o = 1.222 KB	k = 0.001 KB	γ = 0.15
K_1 = 8.0	c = 2.5 KB	$J_{1,LIQ}$ = 12 KB
K_2 = 0.07(KB)$^{-1}$	(ν_o = 0.32)*)	(E_o = 1.3200 KB)

*) Only two of the four constants, K_o, G_o, ν_o, and E_o are independent.

Figure (8) shows the curve of the axial stress σ_1 versus the axial strain ε_1 for a complete loading-unloading cycle for the uniaxial strain configuration. Figure (9) shows the lateral stress σ_3 versus the axial stress σ_1 in uniaxial strain. It is seen that both curves give the characteristic shape of the experimental results, Figs. (1a)-(1b).

A series of ground shock calculations using the three-dimensional (two-dimensional space-time) alluvium-playa model have been made for a model configuration in which (a) the same constant shear modulus $G = G_o$ has been used in both loading and unloading, and (b) the yield condition of Eq. (II-1) has been used, but a plastic potential of the form $\sqrt{J_2'} - k = 0$ has been used in computing the plastic strains, so as to avoid the dilation problems which occur on loading and unloading as described in some detail in Section I.

The effect of using $G = G_o$ in both loading and unloading results in a stress-strain curve for the uniaxial test which although slightly softer in unloading, is essentially the same as the curve in Fig. (8). The lateral stress curve for unloading would differ from the curve shown in Fig. (9), since the unloading and loading curves would coincide at low stresses. The use of the generalized yield condition, Eq. (II-1), together with a plastic potential which is independent of J_1, results in a slightly softer stress-strain curve than is shown in Fig. (8).

It is of interest to consider the behavior of plastic material models of this general type in the triaxial compression test. Figure (10) shows a sketch of a typical $\sigma_1 - \sigma_3$ versus ε_1 diagram. Because of the variable bulk modulus K(p), the initial loading case first softens and then hardens. As the yield surface is reached (at different levels for different values of the lateral stress σ_3), the material "fails" and "flows" along the horizontal lines shown parallel to the strain axis. It is apparent that plastic models of this type in which a constant shear modulus G is used do not mirror the usual stress-strain curves from a triaxial compression test.

A way to remedy this situation is an approach in which variable moduli are used for both K and G. This approach is discussed in detail for several cases in Section III.

III VARIABLE MODULI MATERIAL MODELS.

This section describes the development of the variable moduli models in which no explicit plastic yield condition is specified. As mentioned in the Introduction, these models are an alternate to the approach utilizing plastic yield conditions as described in Sections I and II. In the variable moduli models, both the shear modulus and the bulk modulus will be assumed to depend upon the stress and/or strain invariants.

The mathematical description of the model is in terms of the incremental stress-strain relations

$$\dot{s}_{ij} = 2G\,\dot{e}_{ij} \qquad \text{(III-1)}$$

$$\dot{p} = 3K\,\dot{e} \qquad \text{(III-2)}$$

where s_{ij} and e_{ij} are the deviatoric stress and strain, respectively, and p and e*) are the mean stress and strain. In general, different functions G and K apply in initial loading and subsequent unloading and reloading. The present discussion will be largely confined to the case of initial loading.

It is noted that, even in cases of initial loading, there is not in general a unique stress-strain relation. The final state of strain depends not only upon the final state of stress, but also upon the stress path used to reach

---

*) In this section compressive stress and strain are defined as positive in accordance with the usual soil mechanics convention.

the final state. In this sense, the variable moduli material cannot be considered a nonlinear elastic material where such a unique stress-strain relation would exist. Three different models of this type are discussed in this section: (1) a model in which Poisson's ratio is kept constant; (2) a model in which both K and G are given as a function of the strain tensor invariants, and (3) an essentially equivalent model to (2) in which K is a function of the strain tensor invariants and G is a function of the stress tensor invariants. The latter model is more convenient for large computer codes since it requires less storage capacity per computation point than does the model of type (2).

Each of these models will be discussed from the standpoint of the uniaxial strain and triaxial compression tests, since these are the soil tests which will generally be available for the determination of the material constants for the three-dimensional (two-dimensional space-time) codes. It should be noted that when such models are run for the simple geometries of these two material tests, it is a necessary condition that the experimental test results be closely checked by the mathematical computations. It will be shown that the constant Poisson's ratio model of type (1) cannot match both the uniaxial strain and the triaxial compression experimental results, but that both of the models of type (2) or type (3) do match both tests, and consequently, appear to be suitable mathematical material models.

(1) Constant Poisson's Ratio Model.

A simple variable moduli model which has been suggested and used by some investigators is one in which the ratio $\frac{K}{G}$ remains constant. It will be shown here that a model of this type cannot satisfy both the uniaxial strain and the triaxial compression test results.

By analogy with the linearly elastic relation

$$\frac{K}{G} = \frac{2(1+\nu)}{3(1-2\nu)} \tag{III-3}$$

this model may be called a constant Poisson's ratio material.

However, K and G will not be constants, but functions of the mean strain e

$$\begin{aligned} K &= K(e) \\ G &= G(e) = \frac{3}{\beta} K(e) \end{aligned} \tag{III-4}$$

where β is a constant. Alternatively, K and G may be viewed as functions of the pressure p. Since for initial loading, the pressure

$$p = \int_0^e 3K(\xi)\, d\xi \tag{III-5}$$

is a monotonic function of e, a unique inverse e(p) exists. Thus, the moduli K and G may also be written as

$$\begin{aligned} K &= K(p) = K[e(p)] \\ G &= G(p) = \frac{3}{\beta} K[e(p)] \end{aligned} \tag{III-6}$$

(a) Uniaxial Strain.

In general, the strain increment may be written as

$$\dot{\varepsilon}_{ij} = \frac{\dot{s}_{ij}}{2G} + \frac{\dot{p}\delta_{ij}}{3K} \qquad \text{(III-7)}$$

In the case of uniaxial strain $\dot{s}_2 = \dot{s}_3 = -\frac{\dot{s}_1}{2}$ and

$$\dot{\varepsilon}_2 = \dot{\varepsilon}_3 = -\frac{\dot{s}_1}{4G} + \frac{\dot{p}}{3K} = 0 \qquad \text{(III-8)}$$

Thus,

$$\dot{s}_1 = \frac{4G}{3K}\dot{p} = \frac{4}{\beta}\dot{p} \qquad \text{(III-9)}$$

$$\dot{\varepsilon}_1 = \frac{\dot{s}_1}{2G} + \frac{\dot{p}}{3K} = \frac{\dot{\lambda}}{K} \qquad \text{(III-10)}$$

and

$$\dot{\sigma}_1 = \dot{s}_1 + \dot{p} = (\frac{4}{\beta} + 1)\dot{p} \qquad \text{(III-11)}$$

Combining Eqs. (III-10)and (III-11) leads to the relation

$$\frac{d\sigma_1}{d\varepsilon_1} = (\frac{4}{\beta} + 1) K(\frac{\varepsilon_1}{3}) \qquad \text{(III-12)}$$

The lateral stress is found from the relation

$$\dot{\sigma}_3 = -\frac{\dot{s}_1}{2} + \dot{p} = (-\frac{2}{\beta} + 1)\dot{p} \qquad \text{(III-13)}$$

or

$$\frac{d\sigma_3}{d\varepsilon_1} = (1 - \frac{2}{\beta}) K(\frac{\varepsilon_1}{3}) \qquad \text{(III-14)}$$

Integrating Eq. (III-12) and Eq. (III-14), the expressions for the principal stresses σ_1 and σ_3 become:

$$\sigma_1(\varepsilon_1) = (1 + \frac{4}{\beta}) \int_0^{\varepsilon_1} K(\frac{\xi}{3})\, d\xi \qquad \text{(III-15)}$$

$$\sigma_3(\varepsilon_1) = (1 - \frac{2}{\beta}) \int_0^{\varepsilon_1} K(\frac{\xi}{3})\, d\xi \qquad \text{(III-16)}$$

Equations (III-12), (III-15), and (III-16) define a constant Poisson's ratio material during initial loading in a uniaxial strain configuration. If K(e) initially decreases and subsequently increases, the axial stress - axial strain curve [see Eq. (III-12)] will have the characteristic softening-hardening shape found experimentally, Fig. (1a).

From Eqs. (III-15) and (III-16),

$$\sigma_3(\varepsilon_1) = (\frac{\beta-2}{\beta+4})\, \sigma_1(\varepsilon_1) \qquad \text{(III-17)}$$

so that the radial stress versus axial stress relation is a straight line of slope $\frac{\nu}{1-\nu}$. This agrees reasonably well with experimental data, Fig. (1b).

(b) Triaxial Stress.

In the triaxial test, $\dot{s}_2 = \dot{s}_3 = -\frac{\dot{s}_1}{2}$ and

$$\dot{\sigma}_3 = -\frac{\dot{s}_1}{2} + \dot{p} = 0 \qquad \text{(III-18)}$$

Thus, $\dot{s}_1 = 2\dot{p}$ and $\dot{\sigma}_1 = 3\dot{p}$. The axial strain increment is given by

$$\dot{\varepsilon}_1 = \frac{\dot{s}_1}{2G} + \frac{\dot{p}}{3K} = \left(\frac{1}{G} + \frac{1}{3K}\right) \frac{\dot{\sigma}_1}{3} \qquad \text{(III-19)}$$

and the slope of the stress-strain curve by,

$$\frac{d\sigma_1}{d\varepsilon_1} = \frac{9}{\beta+1} K(e) \qquad \text{(III-20)}$$

The radial strain increment is

$$\dot{\varepsilon}_3 = -\frac{\dot{s}_1}{4G} + \frac{\dot{p}}{3K} = \left(-\frac{1}{2G} + \frac{1}{3K}\right) \frac{\dot{\sigma}_1}{3} \qquad \text{(III-21)}$$

or

$$\dot{\varepsilon}_3 = \frac{-(\beta-2)}{2(\beta+1)} \dot{\varepsilon}_1 = -\nu\dot{\varepsilon}_1 \qquad \text{(III-22)}$$

which, not surprisingly, is the same as the linear elastic relation. The mean strain increment is also proportional to $\dot{\varepsilon}_1$,

$$\dot{e} = \frac{1}{3}\left[\dot{\varepsilon}_1 + 2\dot{\varepsilon}_3\right] = \frac{1}{\beta+1} \dot{\varepsilon}_1 \qquad \text{(III-23)}$$

so that the actual total mean strain is given by

$$e = e_o + \frac{1}{\beta+1} \Delta\varepsilon_1 \qquad \text{(III-24)}$$

where e_o is the strain reached during the loading of the specimen hydrostatically up to the stress σ_3, and where $\Delta\varepsilon_1 = \varepsilon_1 - e_o$ is the measured axial strain.

Typical experimental triaxial results, Fig. (1c), have the following characteristics:

1. The stress-strain curve at a given value of σ_3 is concave downward.
2. At some point a horizontal tangent, "failure", is reached.
3. At a higher value of σ_3 the initial slope and the stress difference at failure, $(\sigma_1 - \sigma_3)_{max}$, both increase.

From Eqs. (III-20) and (III-24) one sees that the requirement of negative curvature $\frac{d^2\sigma_1}{d\varepsilon_1^2} < 0$ means that $\frac{dK}{de}$ must be negative, which contradicts the behavior of K(e) which was required for the uniaxial test. Moreover, the assumption $K > 0$ is not compatible with the existence of "failure" $(\frac{d\sigma_1}{d\varepsilon_1} = 0)$.

Even if a yield condition of some type were included in the model specification, well below the yield point, negative curvature would require $\frac{dK}{de} < 0$. On the other hand, requiring the initial slope to increase with σ_3, or

$$\left.\frac{d^2\sigma_1}{d\varepsilon_1 d\sigma_3}\right]_{\Delta\varepsilon_1=0} = \left.\frac{9}{\beta+1}\frac{dK}{de}\right]_{e=e_o}\left.\frac{de}{dp}\right]_{p=\sigma_3} - \left.\frac{3}{(\beta+1)K}\frac{dK}{de}\right]_{e=e_o} > 0 \qquad \text{(III-25)}$$

requires that $\frac{dK}{de} > 0$, which contradicts the requirement that $\frac{dK}{de} < 0$.

One may therefore conclude that, although the constant Poisson's ratio model appears promising when only the uniaxial

results are considered, such a model must be rejected, even in conjunction with a yield condition, since its behavior in the triaxial configuration contradicts experimental evidence.

(2) Moduli Dependent Upon Strain Invariants.

Models in which the moduli were assumed to be independent functions of the first and second invariants of the strain were investigated in the order of increasing complexity. Initially, strain rather than stress was chosen for analytic convenience, at least with the simpler models.

The most promising of the strain models thus far considered is defined by the relations

$$K = K(e) = K_o + K_1 e + K_2 e^2 \qquad \text{(III-26)}$$

$$G = G(e, \sqrt{I_2'}) = G_o + \bar{G}_1 \sqrt{I_2'} + G_1 e \qquad \text{(III-27)}$$

where I_2' is the second invariant of the strain deviators. Equations (III-26) and (III-27) may be thought of as the first terms in the series expansions of more general analytic functions K and G of the strain invariants. The quantity $\sqrt{I_2'}$ was used, rather than I_2' itself, since it is of the same order as e and the components of the strain tensor. At zero strain, the bulk and shear moduli reduce respectively to K_o and G_o, the "linear elastic" values, which are related in terms of the "elastic" Poisson's ratio ν_o

$$\frac{K_o}{G_o} = \frac{2(1+\nu_o)}{3(1-2\nu_o)} \qquad \text{(III-28)}$$

although the ratio $\frac{K}{G}$ is not, in general, constant. With G_1 positive and $\bar{G}_1$ negative, the material hardens in shear with increasing hydrostatic strain and softens with increasing shear strain.

(a) Uniaxial Strain.

The general incremental stress-strain relation is given by

$$\dot{\varepsilon}_{ij} = \frac{\dot{s}_{ij}}{2[G_o + \bar{G}_1 \sqrt{I_2'} + G_1 e]} + \frac{\dot{p}\delta_{ij}}{3[K_o + K_1 e + K_2 e^2]} \qquad \text{(III-29)}$$

In the case of uniaxial strain, $\dot{s}_2 = \dot{s}_3 = -\frac{\dot{s}_1}{2}$, so that

$$\dot{\varepsilon}_3 = \frac{-\dot{s}_1}{4[G_o + \bar{G}_1 \sqrt{I_2'} + G_1 e]} + \frac{\dot{p}}{3[K_o + K_1 e + K_2 e^2]} = 0 \qquad \text{(III-30)}$$

$$\sqrt{I_2'} = \frac{\sqrt{3}}{2} e_1 \qquad \text{(III-31)}$$

(since in loading $e_1 > 0$) and,

$$e_1 = 2e = \frac{2}{3} \varepsilon_1 \qquad \text{(III-32)}$$

Combining Eqs. (III-30) - (III-32) one obtains an expression for the tangent modulus at any strain

$$\frac{d\sigma_1}{d\varepsilon_1} = [K_o + \frac{K_1}{3} \varepsilon_1 + \frac{K_2}{9} \varepsilon_1^2] + \frac{4}{3} [G_o + \frac{1}{3} (G_1 + \sqrt{3}\, \bar{G}_1)\, \varepsilon_1] =$$

$$= K + \frac{4}{3} G = M \qquad \text{(III-33)}$$

Integrating Eq. (III-33) and combining terms, the axial stress is obtained in closed form as

$$\sigma_1 = [K_o + \frac{4}{3} G_o] \varepsilon_1 + \frac{1}{6} [K_1 + \frac{4}{3} (G_1 + \sqrt{3} \bar{G}_1)] \varepsilon_1^2 + \frac{K_2}{27} \varepsilon_1^3 \quad \text{(III-34)}$$

Noting that $s_3 = -\frac{1}{2} s_1$, the lateral stress at any strain may also be written in closed form as

$$\sigma_3 = [K_o - \frac{2}{3} G_o] \varepsilon_1 + \frac{1}{6} [K_1 - \frac{2}{3} (G_1 + \sqrt{3} \bar{G}_1)] \varepsilon_1^2 + \frac{K_2}{27} \varepsilon_1^3 \quad \text{(III-35)}$$

The pressure is given by the relation

$$p = \frac{1}{3} (\sigma_1 + 2\sigma_3) = K_o \varepsilon_1 + \frac{K_1}{6} \varepsilon_1^2 + \frac{K_2}{27} \varepsilon_1^3 \quad \text{(III-36)}$$

and the deviator s_1 as

$$s_1 = \sigma_1 - p = \frac{4}{3} G_o \varepsilon_1 + \frac{2}{9} (G_1 + \sqrt{3} \bar{G}_1) \varepsilon_1^2 \quad \text{(III-37)}$$

(b) Triaxial Stress.

During triaxial loading, the lateral stress is held constant, so that

$$\dot{\sigma}_3 = -\frac{\dot{s}_1}{2} + \dot{p} = -[G_o + G_1 e + \bar{G}_1 \sqrt{I_2'}] \dot{e}_1 + \\ + 3[K_o + K_1 e + K_2 e^2] \dot{e} = 0 \quad \text{(III-38)}$$

Thus,

$$\dot{s}_1 = 2\dot{p} = \frac{2}{3} \dot{\sigma}_1 \quad \text{(III-39)}$$

and since $\sqrt{I_2'} = \frac{\sqrt{3}}{2} e_1$ (during loading $e_1 > 0$), the strain rate $\dot{e}_1$ is given by

$$\dot{e}_1 = \frac{3[K_o + K_1 e + K_2 e^2]}{[G_o + G_1 e + \frac{\sqrt{3}}{2} \bar{G}_1 e_1]} \dot{e} \qquad \text{(III-40)}$$

The total axial strain increment is given by

$$\dot{\varepsilon}_1 = \dot{e}_1 + \dot{e} \qquad \text{(III-41)}$$

Combining Eqs. (III-39) and (III-40), the tangent modulus is obtained as

$$\frac{d\sigma_1}{d\varepsilon_1} = \frac{9[K_o + K_1 e + K_2 e^2][G_o + G_1 e + \frac{\sqrt{3}}{2} \bar{G}_1 e_1]}{3[K_o + K_1 e + K_2 e^2] + [G_o + G_1 e + \frac{\sqrt{3}}{2} \bar{G}_1 e_1]} \qquad \text{(III-42)}$$

or

$$\frac{d\sigma_1}{d\varepsilon_1} = \frac{9K(e)\, G(e,e_1)}{3K(e) + G(e,e_1)} \equiv E(e,e_1) \qquad \text{(III-43)}$$

where E may be considered the local modulus of elasticity, i.e., Young's modulus.

Equations (III-40) - (III-42) consitute a system of nonlinear differential equations relating the variables e, e_1, ε_1, and σ_1. The system may be solved numerically by forward integration. The initial conditions are obtained from the hydrostatic state of stress which exists in a triaxial compression test before the additional axial loading is applied, namely,

$$\sigma_1(0) = \sigma_3$$

$$e_1(0) = 0 \qquad \text{(III-44)}$$

$$\varepsilon_1(0) = e(0) = e_o$$

where e_o , one third of the hydrostatic volumetric strain, is the small positive root of the cubic equation

$$\sigma_3 = 3K_o e_o + \frac{3}{2} K_1 e_o^2 + K_2 e_o^3 \qquad \text{(III-45)}$$

Since K is always positive, σ_3 increases monotonically with e_o .

(c) Choice of Constants.

If all stress quantities are nondimensionalized with respect to the initial bulk modulus, K_o , then five parameters remain to fully describe the model, namely,

$$\frac{G_o}{K_o} , \frac{K_1}{K_o} , \frac{G_1}{K_o} , \frac{\bar{G}_1}{K_o} , \frac{K_2}{K_o} \qquad \text{(III-46)}$$

The first of these is inherently positive and is related to the initial Poisson's ratio ν_o by Eq. (III-28). The higher order terms in the bulk modulus $\frac{K_1}{K_o}$ and $\frac{K_2}{K_o}$ may be positive or negative. However, the values are restricted by the condition $K > 0$. Taking the derivative of Eq. (III-26) one finds the minimum K occurs at $e_{min} = -\frac{K_1}{2K_2}$, which is positive (i.e., relevant) only for K_1 and K_2 of opposite sign.

If K_2 is taken to be negative, $\frac{-K_1}{2K_2}$ would be the value of e at which K would reach a maximum. With K_1 negative

and K_2 positive, the requirement that the minimum bulk modulus be positive

$$K_{min} = K(e_{min}) = K_o - \frac{K_1^2}{4K_2} > 0 \qquad \text{(III-47)}$$

requires that

$$K_2 > \frac{K_1^2}{4K_o} \qquad \text{(III-48)}$$

It should be noted that any values of $\frac{K_1}{K_o}$ and $\frac{K_2}{K_o}$ are permitted as long as $K > 0$ for the range of e of interest, especially $0 < e < \frac{1}{3}$.

In the triaxial stress test the initial slope

$$\left.\frac{d\sigma_1}{d\varepsilon_1}\right|_{\substack{e_1=0 \\ e=e_o}} = \frac{9[K_c + K_1 e_o + K_2 e_o^2][G_o + G_1 e_o]}{3[K_o + K_1 e_o + K_2 e_o^2] + [G_o + G_1 e_o]} =$$

$$= \frac{9K(e_o)\, G(e_o,0)}{3K(e_o) + G(e_o,0)} \qquad \text{(III-49)}$$

should increase with increasing lateral stress (or e_o). This leads to the relation

$$3[K(e_o)]^2 G_1 + [G(e_o,0)]^2(K_1 + 2K_2 e_o) > 0 \qquad \text{(III-50)}$$

which, for e_o sufficiently small, becomes

$$\frac{G_1}{K_o} + \frac{1}{3}\left(\frac{G_o}{K_o}\right)^2 \frac{K_1}{K_o} > 0 \qquad \text{(III-51)}$$

With $K_1 < 0$, Eq. (III-51) sets a lower bound for G_1 .

In the uniaxial strain test the curvature

$$\frac{dM}{d\varepsilon_1} = \frac{1}{3}\left[K_1 + \frac{4}{3}\left(G_1 + \sqrt{3}\,\bar{G}_1\right)\right] + \frac{2}{9}K_2\varepsilon_1 \qquad \text{(III-52)}$$

is initially negative, or

$$K_1 + \frac{4}{3}\left(G_1 + \sqrt{3}\,\bar{G}_1\right) < 0 \qquad \text{(III-53)}$$

and the curvature changes sign at the inflection point defined by

$$\varepsilon_{1_{\text{inflection point}}} = -\frac{3}{2K_2}\left[K_1 + \frac{4}{3}\left(G_1 + \sqrt{3}\,\bar{G}_1\right)\right] \qquad \text{(III-54)}$$

Equation (III-53) sets an upper bound on $\bar{G}_1$, while Eq. (III-54) relates $K_2 > 0$ to the inflection point once K_1, G_1, and $\bar{G}_1$ are known. The minimum slope (at the inflection point)

$$M_{min} = \left(K_o + \frac{4}{3}G_o\right) - \frac{\left[K_1 + \frac{4}{3}\left(G_1 + \sqrt{3}\,\bar{G}_1\right)\right]^2}{4K_2} \qquad \text{(III-55)}$$

must be positive, so that

$$K_2 > \frac{\left[K_1 + \frac{4}{3}\left(G_1 + \sqrt{3}\,\bar{G}_1\right)\right]^2}{4\left(K_o + \frac{4}{3}G_o\right)} \qquad \text{(III-56)}$$

In practical application of this model to experimental curves, the various constants are chosen by curve-fitting routines to best match the data. For a purely theoretical investigation in which no specific real material is considered, $\frac{G_o}{K_o}$ is obtained from a reasonable value of ν_o, a

value $\frac{K_1}{K_o} < 0$ is chosen, $\frac{G_1}{K_o}$ is taken to satisfy Eq. (III-51), and $\frac{\bar{G}_1}{K_o}$ to satisfy Eq. (III-53). Finally, $\frac{K_2}{K_o}$ is chosen to satisfy both Eqs. (III-48) and (III-56). It is seen that the salient features of both the uniaxial strain compression test and the triaxial compression test can be matched by material models of this type.

(d) Numerical Results.

Typical numerical results were obtained for the parameters $\nu_o = 0.30$, $\frac{K_1}{K_o} = -100$, $\frac{K_2}{K_o} = 4000$, $\frac{G_1}{K_o} = 48$ and $\frac{\bar{G}_1}{K_o} = -32$. For the uniaxial compression test, the plot of axial stress versus axial strain, Fig. (11), shows the reversal in curvature which is characteristic of the experimental curves. The point of inflection occurs at 4.1% strain, again a typical experimental value The plot of the radial stress σ_3 required to maintain uniaxial strain versus axial stress σ_1 is shown in Fig. (12). The general trend of this curve conforms to the experimental curve, Fig. (1b). It may be noted that a slight reverse curvature occurs at the low end of the theoretical curve. Although a change in the material parameters could alter or possibly remove this effect at the low end, it is not completely clear as to whether such effects occur in some real materials. In any case, this effect is a minor one and is not sufficient grounds for rejecting the model. Figure (13) is a plot of the deviator $\frac{s_1}{K_o}$ versus the pressure $\frac{p}{K_o}$, again for uniaxial

strain. Once more, at the low end there is a reverse in curvature. However, beyond the inflection point, the slope of the curve is remarkably similar to the curve of the playa-type yield condition, described in Fig. (4). More will be said about the similarities and differences between the plastic and variable moduli models later.

In the triaxial test, the stress difference $\sigma_1 - \sigma_3$ versus the axial strain ε_1 is shown in Fig. (14) for the same constants that were used in the uniaxial calculation, and for $\frac{\sigma_3}{K_o} = 0.04, 0.06, 0.08$, respectively. The curves are found by the numerical integration of Eqs. (III-40) - (III-42) and reflect the experimental results, Fig. (1c). The curves are concave downward, exhibit horizontal tangents, "failure", and at higher lateral stresses the initial slope increases and the stress difference at "failure" increases.

Since an analytical expression for the stress difference at failure is unattainable, the computer program was run to failure for nine different values of the lateral stress, σ_3. Table I shows the stress difference, the pressure, and the axial strain at failure as well as the initial modulus for each value of lateral stress. The Mohr envelope is plotted in Fig. (15). Again, there is overall agreement with experimental envelopes, Fig. (1d), except for a small discrepancy at very low stresses.

TABLE I

Triaxial Test at Various Lateral Stresses

$(\nu_o = 0.30,\ \frac{K_1}{K_o} = -100,\ \frac{K_2}{K_o} = 4000,\ \frac{G_1}{K_o} = 48,\ \frac{\bar{G}_1}{K_o} = -32)$

No.	$\frac{\sigma_3}{K_o}$	$\frac{(\sigma_1-\sigma_3)_{failure}}{K_o}$	$\frac{p_{failure}}{K_o}$	$\epsilon_{1_{failure}}$	$\frac{E_{initial}}{K_o}$
1	0.000	0.0139	0.0046	0.0211	1.200
2	0.001	0.0153	0.0061	0.0232	1.231
3	0.005	0.0230	0.0126	0.0317	1.350
4	0.010	0.0577	0.0292	0.0667	1.479
5	0.020	0.1608	0.0736	0.1045	1.594
6	0.040	0.2385	0.1195	0.1212	2.977
7	0.060	0.2819	0.1540	0.1310	3.973
8	0.080	0.3162	0.1854	0.1374	4.625
9	0.100	0.3456	0.2152	0.1426	5.117

On the basis of the present investigation, it appears that the variable moduli model under consideration, defined by Eqs. (III-26) and (III-27), shows promise as a mathematical representation of the mechanical behavior of soils. The model behavior in both uniaxial strain and triaxial stress configurations (in initial loading) is essentially similar to that found experimentally.

No attempt was made to use this model to match actual data numerically, nor was the problem of unloading given more than a cursory glance. These activities were postponed in order to develop a variable moduli model which depends upon the stress invariants p and $\sqrt{J_2'}$ as well as the mean strain e*). This was done for practical as well as theoretical reasons. Practically, in the general three-dimensional problem, one is physically more interested in stresses than strains and already stores the stresses in the computer. To require the storage of even a single extra quantity at each grid point significantly reduces the number of grid points which can be utilized.

From a theoretical viewpoint, this stress invariant model allows an interesting comparison with plastic models which will be discussed later.

---

*) In the various computer codes for evaluating ground shock, the density ρ is generally stored at each point and the mean strain e may be computed from it.

(3) Combined Stress-Strain Variable Moduli Model.

This section presents the development of a material model in which the bulk modulus K is a function of the mean strain e, and the shear modulus G is a function of the stress tensor invariants, through the mean pressure p and the square root of the second invariant of the stress deviator $\sqrt{J_2'}$.

The simplest relation in which the shear modulus depends upon both p and $\sqrt{J_2'}$ is given by

$$G = G_o + \gamma_1 p + \bar{\gamma}_1 \sqrt{J_2'} \qquad \text{(III-57)}$$

The bulk modulus is retained as a quadratic function of the volumetric strain

$$K = K_o + K_1 e + K_2 e^2 \qquad \text{(See Eq. III-26)}$$

As mentioned in Section III-1 for the constant Poisson's ratio model, a unique pressure-volumetric strain relation exists during initial loading as long as the bulk modulus depends only upon p or e. Therefore, Eq. (III-26) is equivalent to writing K as a function of p [See Eq. (III-6)].

The bulk modulus was chosen to be a quadratic in e rather than in p, since the typical uniaxial strain test curve suggests that the axial stress is a cubic function of the axial strain. Since the moduli K and G refer to the incremental stress-strain relations,

$$\dot{p} = 3K\,\dot{e} \qquad \text{(See Eq. III-1)}$$

$$\dot{s}_{ij} = 2G\,\dot{e}_{ij} \qquad \text{(See Eq. III-2)}$$

the pressure may be obtained by direct integration of Eq. (III-1) as

$$p = \int_0^e 3K(\xi)\,d\xi = 3K_o e + \frac{3}{2}K_1 e^2 + K_2 e^3 \qquad \text{(III-58)}$$

Moreover, in the preparation of a computer code for the solution of three-dimensional (two-dimensional space-time) ground shock problems, the density (or the volumetric strain ε_{kk}) must be stored at each grid point, since the density appears in the equations of motion. Since the relation between density and volumetric strain is given by

$$\varepsilon_{kk} = 3e = \ln\left(\frac{\rho}{\rho_o}\right) \qquad \text{(III-59)}$$

it is noted that the use of a bulk modulus which is a function of the mean strain, Eq. (III-26), requires no significant additional computer storage*). It should also be noted that in Eq. (III-57), the nondimensional constant γ_1 will be positive for a G which hardens with increasing pressure, while $\bar{\gamma}_1$ will be negative for a G which softens with an increase in the deviatoric stresses.

---

*) In the large ground shock problems, the problem of minimizing computer storage requirements at each grid point becomes extremely important, since the size of the problems challenges the capacity of even the largest computers.

(a) Uniaxial Strain.

In a manner quite analogous to the case of the strain invariant model, Section III-2, it may be shown that in uniaxial strain

$$\frac{d\sigma_1}{de} = 3K + 4G = 3[K_o + K_1 e + K_2 e^2] + 4[G_o + \gamma_1 p + \bar{\gamma}_1 \sqrt{J_2}] \quad \text{(III-60)}$$

Noting that $\sqrt{J_2} = \frac{\sqrt{3}}{2} s_1 = \frac{\sqrt{3}}{2} (\sigma_1 - p)$, substitution of Eq. (III-58) into Eq. (III-60) yields the first order non-homogeneous differential equation

$$\frac{d\sigma_1}{de} - 2\sqrt{3}\,\bar{\gamma}_1\,\sigma_1 = (3K_o + 4G_o) + 3[4K_o(\gamma_1 - \tfrac{\sqrt{3}}{2}\bar{\gamma}_1) + K_1]\,e +$$

$$+ 3[2K_1(\gamma_1 - \tfrac{\sqrt{3}}{2}\bar{\gamma}_1) + K_2]\,e^2 + 4K_2(\gamma_1 - \tfrac{\sqrt{3}}{2}\bar{\gamma}_1)\,e^3 \quad \text{(III-61)}$$

Using the initial condition that stress and strain vanish simultaneously, the solution for stress as an explicit function of strain is found by integrating Eq. (III-61)

$$\sigma_1 = -\left\{ \frac{2G_o}{\sqrt{3}\,\bar{\gamma}_1} + \frac{\gamma_1}{\bar{\gamma}_1^2}\left[K_o + \frac{K_1}{2\sqrt{3}\,\bar{\gamma}_1} + \frac{2K_2}{(2\sqrt{3}\,\bar{\gamma}_1)^2}\right]\right\}\left[1 - \exp(2\sqrt{3}\,\bar{\gamma}_1 e)\right] -$$

$$- \left\{ \frac{2\sqrt{3}\,K_o}{\bar{\gamma}_1}(\gamma_1 - \tfrac{\sqrt{3}}{2}\bar{\gamma}_1) + \frac{\gamma_1}{\bar{\gamma}_1^2}(K_1 + \frac{K_2}{\sqrt{3}\,\bar{\gamma}_1}) \right\} e -$$

$$- \left\{ \frac{\sqrt{3}\,K_1}{\bar{\gamma}_1}(\gamma_1 - \tfrac{\sqrt{3}}{2}\bar{\gamma}_1) + \frac{\gamma_1}{\bar{\gamma}_1^2} K_2 \right\} e^2 - \frac{2K_2}{\sqrt{3}\,\bar{\gamma}_1}(\gamma_1 - \tfrac{\sqrt{3}}{2}\bar{\gamma}_1)\,e^3$$

(III-62)

Closed form expressions for the remaining stress quantities, s_1 and σ_3, are easily obtainable from Eqs. (III-58) and (III-62).

$$s_1 = -\left\{\frac{2G_o}{\sqrt{3}\,\bar{\gamma}_1} + \frac{\gamma_1}{\bar{\gamma}_1^2}\left[K_o + \frac{K_1}{2\sqrt{3}\,\bar{\gamma}_1} + \frac{2K_2}{(2\sqrt{3}\,\bar{\gamma}_1)^2}\right]\right\}\left[1 - \exp(2\sqrt{3}\,\bar{\gamma}_1 e)\right] -$$

$$- \left[\frac{2\sqrt{3}\,\gamma_1}{\bar{\gamma}_1} K_o + \frac{\gamma_1}{\bar{\gamma}_1^2}\left(K_1 + \frac{K_2}{\sqrt{3}\,\bar{\gamma}_1}\right)\right] e -$$

$$- \left[\frac{\sqrt{3}\,\gamma_1}{\bar{\gamma}_1} K_1 + \frac{\gamma_1}{\bar{\gamma}_1^2} K_2\right] e^2 - \frac{2\gamma_1}{\sqrt{3}\,\bar{\gamma}_1} K_2\, e^3 \qquad \text{(III-63)}$$

$$\sigma_3 = \left\{\frac{G_o}{\sqrt{3}\,\bar{\gamma}_1} + \frac{\gamma_1}{2\bar{\gamma}_1^2}\left[K_o + \frac{K_1}{2\sqrt{3}\,\bar{\gamma}_1} + \frac{2K_2}{(2\sqrt{3}\,\bar{\gamma}_1)^2}\right]\right\}\left[1 - \exp(2\sqrt{3}\,\bar{\gamma}_1 e)\right] +$$

$$+ \left[\frac{\sqrt{3}\,K_o}{\bar{\gamma}_i}(\gamma_1 + \sqrt{3}\,\bar{\gamma}_1) + \frac{\gamma_1}{2\bar{\gamma}_1^2}\left(K_1 + \frac{K_2}{\sqrt{3}\,\bar{\gamma}_1}\right)\right] e +$$

$$+ \left[\frac{\sqrt{3}\,K_1}{2\bar{\gamma}_1}(\gamma_1 + \sqrt{3}\,\bar{\gamma}_1) + \frac{\gamma_1}{2\bar{\gamma}_1^2} K_2\right] e^2 + \frac{K_2}{\sqrt{3}\,\bar{\gamma}_1}(\gamma_1 + \sqrt{3}\,\bar{\gamma}_1)\, e^3$$

(III-64)

Finally, from Eq. (III-62), the slope of the stress-strain curve at any point, or the tangent (constrained) modulus is found to be

$$\frac{d\sigma_1}{d\varepsilon_1} = \left\{ \frac{4}{3} G_o + \frac{2\gamma_1}{\sqrt{3}\,\bar{\gamma}_1} \left[K_o + \frac{K_1}{2\sqrt{3}\,\bar{\gamma}_1} + \frac{2K_2}{(2\sqrt{3}\,\bar{\gamma}_1)^2} \right] \right\} \exp(2\sqrt{3}\,\bar{\nu}_1 e) -$$

$$- \frac{2K_o}{\sqrt{3}\,\bar{\gamma}_1} \left(\gamma_1 - \frac{\sqrt{3}}{2}\,\bar{\gamma}_1\right) - \frac{\gamma_1}{3\bar{\gamma}_1^2} \left(K_1 + \frac{K_2}{\sqrt{3}\,\bar{\gamma}_1}\right) -$$

$$-\left[\frac{2K_1}{\sqrt{3}\,\bar{\gamma}_1} \left(\gamma_1 - \frac{\sqrt{3}}{2}\,\bar{\gamma}_1\right) + \frac{2\gamma_1}{3\bar{\gamma}_1^2} K_2\right] e - \frac{2K_2}{\sqrt{3}\,\bar{\gamma}_1} \left(\gamma_1 - \frac{\sqrt{3}}{2}\,\bar{\gamma}_1\right) e^2 \qquad \text{(III-65)}$$

(b) Triaxial Stress.

In the triaxial stress configuration the second invariant of the stress deviators is simply related to the stress difference by

$$\sqrt{J_2'} = \frac{\sqrt{3}}{2} s_1 = \frac{1}{\sqrt{3}} (\sigma_1 - \sigma_3) \qquad \text{(III-66)}$$

Using the relation $p = (\sigma_1 + 2\sigma_3)/3$ and Eq. (III-66), the expression for the shear modulus becomes

$$G = G_o + \frac{\gamma_1}{3} (\sigma_1 + 2\sigma_3) + \frac{\bar{\gamma}_1}{\sqrt{3}} (\sigma_1 - \sigma_3) \qquad \text{(III-67)}$$

Thus, the strain deviator e_1 may be found by integration

$$e_1 = \int \frac{ds_1}{2G} = \int_{\sigma_3}^{\sigma_1} \frac{d\xi}{3G_o + \sigma_3(2\gamma_1 - \sqrt{3}\,\bar{\gamma}_1) + \xi(\gamma_1 + \sqrt{3}\,\bar{\gamma}_1)} \qquad \text{(III-68)}$$

since $e_1 = 0$ when $\sigma_1 = \sigma_3$ (hydrostatic compression).

From Eq. (III-68), e_1 is obtained as an explicit function of the stresses σ_1 and σ_3

$$e_1 = \frac{1}{\gamma_1 + \sqrt{3}\,\bar{\gamma}_1} \ln \left[\frac{3G_o + \sigma_3(2\gamma_1 - \sqrt{3}\,\bar{\gamma}_1) + \sigma_1(\gamma_1 + \sqrt{3}\,\bar{\gamma}_1)}{3(G_o + \gamma_1\sigma_3)}\right] \tag{III-69}$$

A necessary condition for G to decrease as σ_1 increases, see Eq. (III-67), is

$$\gamma_1 + \sqrt{3}\,\bar{\gamma}_1 < 0 \tag{III-70}$$

so that the argument of the logarithmic function in Eq. (III-69) is always less than one, and e_1 is always positive. Alternatively, Eq. (III-69) may be written as

$$e_1 = \frac{1}{\gamma_1 + \sqrt{3}\,\bar{\gamma}_1} \ln \left[\frac{G}{G_{initial}}\right] \tag{III-71}$$

where $G_{initial} = G_o + \gamma_1\sigma_3$ is the initial value of G, i.e., the value under hydrostatic conditions. From Eq. (III-71), it is evident that e_1 becomes arbitrarily large (as does ε_1) as G approaches zero, or [from Eq. (III-67)] when

$$(\sigma_1 - \sigma_3)_{max} = -\frac{3(G_o + \gamma_1\sigma_3)}{\gamma_1 + \sqrt{3}\,\bar{\gamma}_1} \tag{III-72}$$

It is seen that for $(\sigma_1 - \sigma_3)$ larger than $(\sigma_1 - \sigma_3)_{max}$, the strain becomes imaginary, that is, the strain cannot exist. Thus, Eq. (III-72) expresses the maximum stress difference in triaxial compression for a given lateral

stress σ_3 . It should also be noted that the local slope of the triaxial stress-strain curve

$$\frac{d\sigma_1}{d\varepsilon_1} = \frac{9KG}{3K + G} \equiv E^{*)} \qquad \text{(See Eq. III-43)}$$

goes to zero when $G \to 0$, so that the stress difference $(\sigma_1 - \sigma_3)_{max}$ represents a point of horizontal tangency, i.e., "failure".

The measured strain $\Delta\varepsilon_1$ is simply related to the strain deviator e_1 , the mean strain e, and the initial (hydrostatic) mean strain e_o by

$$\Delta\varepsilon_1 = e_1 + e - e_o \qquad \text{(III-73)}$$

where e_o is found for the given lateral stress σ_3 by Eq. (III-45). Equations (III-57), (III-26), (III-69), (III-43), (III-73), and the small positive root e of the cubic Eq. (III-58) completely define the system in triaxial stress for all valid stress states σ_1 , σ_3 $[(\sigma_1 - \sigma_3) < (\sigma_1 - \sigma_3)_{max}]$.

If the Mohr failure envelope were plotted fo this material, it is evident from Eq. (III-72) that the plot would be a straight line passing above the origin, similar to the yield condition for a Prager-Drucker material. This similarity will be discussed later in the paper.

---

*) It can be shown that Eq. (III-43) applies for quite general functions K and G.

(c) Choice of Constants.

As for the case of the strain invariant model, Section III-2, five parameters are required to fully describe the material in initial loading:

$$\frac{G_o}{K_o} \ , \ \frac{K_1}{K_o} \ , \ \gamma_1 \ , \ \bar{\gamma}_1 \ , \ \frac{K_2}{K_o} \tag{III-74}$$

The choice of a suitable value of ν_o determines the ratio $\frac{G_o}{K_o}$, Eq. (III-28). The requirement that $K > 0$ again leads to the condition between K_1 and K_2 as given by Eq. (III-48). The fact that $\gamma_1 > 0$ and $\bar{\gamma}_1 < 0$ for physical reasons has already been discussed, as has the inequality between them, Eq. (III-70).

To further restrict the range of the five material parameters, one requires the initial slope in triaxial compression to increase with lateral stress, and the initial curvature in uniaxial strain to be negative. Differentiating Eq. (III-43) with respect to σ_3

$$\frac{1}{9}\frac{dE}{d\sigma_3} = \frac{3K^2\frac{dG}{d\sigma_3} + G^2\frac{dK}{d\sigma_3}}{(3K+G)^2} \tag{III-75}$$

and requiring the result to be positive when $\sigma_1 = \sigma_3$, yields the inequality

$$9\gamma_1 [K_o + K_1 e_o + K_2 e_o^2]^3 +$$

$$+ [G_o + \gamma_1 (3K_o e_o + \frac{3}{2} K_1 e_o^2 + K_2 e_o^3)]^2 (K_1 + 2K_2 e_o) > 0 \qquad \text{(III-76)}$$

For Eq. (III-76) to hold in the limit as e_o approaches zero the inequality

$$\gamma_1 > -\frac{1}{9} \left(\frac{G_o}{K_o}\right)^2 \left(\frac{K_1}{K_o}\right) \qquad \text{(III-77)}$$

must be satisfied. Equation (III-77) is a necessary condition for the initial slope in the triaxial test to increase with increasing lateral stress σ_3 . Requiring the initial curvature in the uniaxial strain test to be negative results in the condition

$$\frac{K_1}{K_o} < -\frac{4}{\sqrt{3}} \bar{\gamma}_1 \left[2 \frac{G_o}{K_o} + \frac{\sqrt{3}\ \gamma_1}{\bar{\gamma}_1}\right] \qquad \text{(III-78)}$$

Equation (III-78) is obtained by evaluating the derivative of Eq. (III-65) at e = 0. An attempt to find an analytic expression for the inflection point leads to a transcendental equation and will not be discussed further.

(d) Unloading.

The model for unloading (and subsequent reloading) of variable moduli materials is presently in the very early stage of development. Thus far, only unloading in the uniaxial strain configuration has been considered. Experimentally, Fig. 1a, the uniaxial strain unloading curve has

a slope much larger than the loading slope, which is approximately constant until very low stress levels are reached.

As a first approach, the material model in unloading was chosen to be defined by the following expressions for the bulk and shear moduli:

$$K = K_{UN} = \text{constant} \tag{III-79}$$

$$G = G_{UN} = G_o + \gamma_1 p + \bar{\gamma}_1 \sqrt{J_2'}\, h(\dot{J}_2') \tag{III-80}$$

where $h(\dot{J}_2')$ is the unit step function. The effect of the step function in Eq. (III-80) is that at the same values of p and J_2', the material is stiffer in shear when it is unloading <u>in shear</u>, $\dot{J}_2' < 0$, than when it is loading in shear, $\dot{J}_2' > 0$. In a completely general three-dimensional configuration the terms "loading" and "unloading" no longer have such clear-cut meanings. It is possible that the material will be loading in shear ($\dot{J}_2' > 0$) and unloading in pressure ($\dot{p} < 0$) simultaneously. In fact, if one studies the $\sigma_3 - \sigma_1$ curve for as simple a geometry as a uniaxial strain test, Fig. (1b), it can be shown that on unloading, the deviator $s_1 = \frac{2}{3}(\sigma_1 - \sigma_3)$ [originally positive] first decreases, then changes sign and continues to decrease [increases negatively] until a minimum is reached at a very low stress level. Beyond this point, s_1 appears to increase slightly, i.e., to decrease in absolute value. At the same

time, the pressure $p = \frac{\sigma_1 + 2\sigma_3}{3}$ and the strain ε_1 both decrease monotonically during unloading. Clearly, the sharp tails found experimentally upon unloading at very low stress levels in both the uniaxial stress-strain curve, Fig. (1a), and the radial stress-axial stress curve, Fig. (1b), are related to this unusual behavior of s_1 .

Plastic models in which the yield condition is a function of J_1 , Eq. (I-4), can adequately represent this behavior*). Presently, the variable moduli model which is described by Eqs. (III-79) - (III-80) in unloading does not adequately describe this behavior at very low stress levels. It is not clear that $\dot{J}_2'$ should be the criterion upon which the choice of the proper G is based. Further study may indicate that some combination of $\dot{J}_2'$ and $\dot{p}$ should be used for this purpose.

The slope of the uniaxial stress-strain curve in unloading, $K_{UN} + \frac{4}{3} G_{UN}$, could not be less than K_{UN} unless G_{UN} were permitted to be negative for some range of stresses. Thus, in order to obtain the sharp break found in the experimental curve, Fig. (1a), at low stress levels, a description of G_{UN} such that it could be negative at very low stress levels appears to be promising. Work on the proper

*) It can be shown that the minimum value of the deviator s_1 occurs when upon unloading, the opposite face of the yield surface is reached. Upon continued unloading, the stress path is along the yield surface.

representation of unloading for variable moduli models is continuing.

For the present model, K_{UN} must be chosen larger than the maximum value of K found during loading. A second requirement is that $\frac{3}{2} K_{UN}$ must be greater than the maximum value of G_{UN} *). Since the work is still in the early stage of development and is subject to revision, a detailed description of the equations applicable to unloading will not be given.

(e) Numerical Results.

Typical results for the variable moduli model of this section are shown in Figs. (16) - (19). The parameters used in the computations were $\nu_o = 0.30$, $\frac{K_1}{K_o} = -100$, and $\frac{K_2}{K_o} = 4000$, the same as were used in the previous strain model. In addition, the values $\gamma_1 = 60$ and $\bar{\gamma} = -133.3$ were chosen. In loading, the uniaxial stress-strain curve, Fig. (16), has the characteristic reversal of curvature which is found in experimental curves. Again, the point of inflection occurs at a strain close to 4%, a typical value. On unloading, with $\frac{K_{UN}}{K_o} = 30$, the stress decreases sharply. Although the unloading portion appears to be a straight line, the slope at low stress levels is in fact less than half the value at high stress levels. Nevertheless, the distinct tail which is found on unloading experimentally, Fig. (1a), does not

*) This corresponds to the requirement $\nu > 0$.

appear, illustrating the inadequacy of the present unloading model at these very low stresses.

The plot of the radial stress versus axial stress in uniaxial strain is shown in Fig. (17). On loading, the curve is actually concave upward at very low stress levels. At higher stresses, the curve is essentially a straight line. The unloading radial stress is always greater than the corresponding value in loading. The unloading curve is concave downward and changes in curvature at $\sigma_1 = 0.164$, where s_1 changes sign. The plot has the same general characteristics as the experimental curves, Fig. (1b), except that in the experimental unloading curve σ_3 drops off much more sharply as σ_1 is brought back to zero.

Finally, the deviator s_1 is plotted versus the pressure p in Fig. (18) for loading and unloading in uniaxial strain. On loading, the initial curvature is concave downward. However, the major portion of the curve is essentially a straight line. On unloading s_1 is always less than its corresponding value in loading and the curve is concave upward. At $s_1 = 0$, the slope is continuous, but the curvature suddenly increases, reflecting the change in sign of $\dot{J}_2'$ in Eq. (III-80). The plot ends at $s_1 = -p$ (so that $\sigma_1 = 0$) with the slope almost horizontal.

The results for the triaxial compression test are illustrated for loading only in Fig. (19). The curves are drawn for the same parameters which were used in the uniaxial

strain test and for the same values of the lateral stress which were used in the strain variable moduli model, Fig. (14), namely $\frac{\sigma_3}{K_o} = 0.04, 0.06, 0.08$. Each of the curves is concave downward and approaches asymptotically the value $(\sigma_1 - \sigma_3)_{max}$ given by Eq. (III-72). At a higher value of the lateral stress, the stress difference at failure increases, as does the initial slope.

On the basis of the present results, one sees that the theoretical combined variable moduli material, when subjected to two special loading configurations, namely the uniaxial strain and triaxial compression test, reproduces all the salient features found experimentally in these tests. Therefore, the present model offers promise of being able to give a reasonable representation of real soils in more general loading configurations.

The tentative unloading model appears to mirror the uniaxial strain experimental results over most of the stress range of interest. Further work is required to clarify the material behavior at very low stresses and to study unloading in the triaxial compression test.

The ability of the present model to match, numerically, real soil data and the process used to determine the various constants must await the completion of current investigations, both theoretical and experimental.

It is of interest to explore in some detail the relation between the variable moduli models in Section III and the various plastic models discussed in Sections I and II. This discussion follows in Part (f).

(f) Comparison of Variable Moduli and Plastic Models.

In the previous portion of this section, sir rities between the variable moduli models and the plastic models have been mentioned. This subsection discusses several of these similarities for simplified models of these types. On the basis of the present study, it appears that the concepts of a "yield condition" and of plastic flow may be contained within the theory of the variable moduli models.

For many materials, empirical evidence suggests the existence of states of stress (and/or strain) at which the material undergoes continuously increasing deformations with little or no increase in loading. This combination of stresses at which flow occurs is often called a "flow condition" or a "yield condition". When these deformations become sufficiently large so that unacceptable changes in the geometry occur, this state is called "failure". Plastic material models describe the stress state at which flow begins by a yield condition and the subsequent deformations by a flow rule. The variable moduli models describe the behavior of materials as they approach this critical state of stress (and/or strain) as well as their behavior at the

state itself. For example, if one were to define an "incremental shear modulus" as the change in shear stress divided by the corresponding change in shear strain and apply this definition to the alluvium-playa model in triaxial compression, Fig. (10), this incremental shear modulus would be zero at "failure". Large increases in shear strain would suddenly occur with no increase in shear stress in this situation. In the case of either of the variable moduli models, Figs. (14), (19), the material does not suddenly fail, but instead gets increasingly softer up to the "failure" point, i.e., G decreases <u>continuously</u> to zero. Examining the behavior of the deviator s_1 for a Coulomb material in uniaxial strain in the very low stress range during unloading (this corresponds to the flat portion of Fig. 2), one finds that s_1 is opposite in sign from σ_1 and becomes smaller in magnitude. The strain deviator, $e_1 = \frac{2}{3}\,\varepsilon_1$ for uniaxial strain, decreases monotonically. Thus, the ratio $\frac{ds_1}{de_1}$ is negative in this region. Although the present unloading relation, Eq. (III-80), does not adequately represent this behavior at low stresses, it is felt that improved versions of the mathematical model in which G on unloading may be negative*) for certain combinations of stresses, may provide a better representation.

An interesting illustration of the relation between plastic and variable moduli models can be obtained by a comparison of the simple Prager-Drucker material and the combined

*) In the present combined variable modulus model, the shear modulus G is necessarily positive in both loading and unloading.

variable moduli material with $K_1 = K_2 = 0$. For both models, the Mohr failure envelope is a straight line. In the Prager-Drucker material, permissible states of stress may be defined in terms of the yield condition

$$k + 3\alpha p - \sqrt{J_2'} \geq 0 \qquad \text{(See Eq. I-1)}$$

In the combined variable moduli material, permissible states of stress are those for which $C \geq 0$, or, dividing Eq. (III-57) by $-\bar{\gamma}_1 > 0$

$$\left(\frac{G_o}{-\bar{\gamma}_1}\right) + \left(\frac{\gamma_1}{-\bar{\gamma}_1}\right) p - \sqrt{J_2'} \geq 0 \qquad \text{(III-81)}$$

The two conditions are identical if

$$\left(\frac{G_o}{-\bar{\gamma}_1}\right) = k \qquad \text{(III-82)}$$

and

$$\left(\frac{\gamma_1}{-\bar{\gamma}_1}\right) = 3\alpha \qquad \text{(III-83)}$$

The requirement that $\gamma_1 + \sqrt{3}\,\bar{\gamma}_1 < 0$, Eq. (III-70), is thus equivalent to requiring that $\alpha < \frac{1}{\sqrt{3}}$. There is no obvious requirement for $\gamma_1 + \frac{\sqrt{3}}{2}\,\bar{\gamma}_1 < 0$, which would correspond to the usual restriction on α*)

$$\alpha < \frac{1}{2\sqrt{3}} \qquad \text{(III-84)}$$

---

*) Equation (III-84) is not an obvious requirement either; it comes either from the restriction $\phi \leq 90^\circ$ in plane strain, or that the slope in uniaxial strain in unloading be positive.

In uniaxial strain, the requirement for initial softening, Eq. (III-78), with $K_1 = 0$ reduces to

$$2 \frac{G_o}{K_o} + \sqrt{3} \frac{\gamma_1}{\bar{\gamma}_1} > 0 \qquad \text{(III-85)}$$

which upon substitution of Eq. (III-83) and $\beta = 3 \frac{K_c}{G_o}$ becomes

$$\alpha\beta < \frac{2}{\sqrt{3}} \qquad \text{(III-86)}$$

The identical condition must be satisfied for a Prager-Drucker material to yield in uniaxial strain.

Finally, examining the slope in uniaxial strain for the combined mixed moduli material, Eq. (III-65), when $K_1 = K_2 = 0$, one finds

$$\frac{d\sigma_1}{d\varepsilon_1} = [\frac{4}{3} G_o + \frac{2}{\sqrt{3}} \frac{\gamma_1}{\bar{\gamma}_1} K_o] \exp(\frac{2}{\sqrt{3}} \bar{\gamma}_1 \varepsilon_1) + K_o(1 - \frac{2}{\sqrt{3}} \frac{\gamma_1}{\bar{\gamma}_1}) \qquad \text{(III-87)}$$

The initial slope, Eq. (III-87) evaluated at $\varepsilon_1 = 0$, is the elastic constrained modulus $K_o + \frac{4}{3} G_o$. At large strains, since $\bar{\gamma}_1 < 0$, the exponential term vanishes and the slope approaches asymptotically

$$\left.\frac{d\sigma_1}{d\varepsilon_1}\right|_{-\bar{\gamma}_1\varepsilon_1 >> 1} = K_o(1 - \frac{2}{\sqrt{3}} \frac{\gamma_1}{\bar{\gamma}_1}) \qquad \text{(III-88)}$$

If the K_1 and K_2 terms were kept in the bulk modulus relation, the slope would simply continue to increase.

In the linear elastic Prager-Drucker material, the slope in uniaxial strain, [see Fig. (2)], is the elastic slope $K_o + \frac{4}{3} G_o$ until yield, at which point the slope becomes discontinuously the plastic slope

$$\left.\frac{d\sigma_1}{d\varepsilon_1}\right]_{\text{Plastic}} = K_o \frac{(1 + 2\sqrt{3}\,\alpha)^2}{(1 + 3\alpha^2\beta)} \qquad \text{(III-89)}$$

The limiting value of the variable moduli slope

$$K_o\left(1 - \frac{2}{\sqrt{3}} \frac{\gamma_1}{\bar{\gamma}_1}\right) = K_o(1 + 2\sqrt{3}\,\alpha) \qquad \text{(III-90)}$$

is not, however, the plastic slope, Eq. (III-89). The two are equal at the end points $\alpha = 0$ and $\alpha = \frac{2}{\beta\sqrt{3}}$ of the range $0 < \alpha < \frac{2}{\beta\sqrt{3}}$, but the variable moduli value is slightly less than the plastic value elsewhere in the range. The value, Eq. (III-90), is that which would be obtained for a hybrid material, i.e., one which obeyed a yield condition of the Coulomb type, but obeyed a flow rule of the von Mises type, [2]. For this material, even incremental dilatancy effects (see Section I) are suppressed. It is not surprising that in a material such as the variable moduli material in which the bulk modulus is a function of the mean strain only and in which shear effects cannot cause an increase in volume, the slope approaches that of the hybrid plastic material and not that of the Coulomb material itself.

Finally, comparing both the triaxial stress and the uniaxial strain tests for the variable moduli material and the

Prager-Drucker material, Fig. (20). one sees that the latter describes yield, while the former describes material behavior approaching "yield".

(4) Closing Remarks.

A theory of variable moduli materials has been partially developed in this section. The results obtained for two of the models appear to essentially match those found experimentally in both the uniaxial strain and triaxial compression tests, at least for some soils in certain ranges of stress. Further work must still be done in unloading. Moreover, as new experimental results become available for higher stress ranges, the extension of the variable moduli models to these higher stress ranges must be examined.

It should be noted that whereas the alluvium-playa model discussed in Section II may be considered to be a relatively advanced plastic model, the variable moduli models presented in this section are a first attempt at such a theory. Further development will hopefully lead to variable moduli models of more general applicability.

REFERENCES

[1] "Soil Mechanics and Plastic Analysis or Limit Design", by D.C. Drucker and W. Prager, Quar. Appl. Math., 1952, Pg. 157.

[2] "Moving Step Load on Half-Space of Granular Material", by Hans H. Bleich and Ewald Heer, Proceedings, A.S.C.E., Vol. 89, No. EM 3, June 1963. [See also "Step Load Moving with Low Subseismic Velocity on the Surface of a Half-Space of Granular Material", by Bleich and Heer, Air Force Special Weapons Center, Technical Documentary Report AFSWC-TDR-63-2, Paul Weidlinger, Consulting Engineer.]

[3] "Step Load Moving on the Surface of a Half-Space of a Locking Material - Subseismic Case", by H.H. Bleich, Paul Weidlinger, Consulting Engineer, Air Force Weapons Laboratory, Technical Documentary Report WL-TDR-64-8, February 1965.

[4] "Step Load Moving with Superseismic Velocity on the Surface of a Half-Space of Granular Material", by H.H. Bleich, A.T. Matthews and J.P. Wright, Paul Weidlinger, Consulting Engineer, Air Force Weapons Laboratory, Technical Report AFWL-TR-65-59, September 1965.

[5] "Exponentially Decaying Pressure Pulse Moving with Superseismic Velocity on the Surface of a Half-Space of Granular Material", by H.H. Bleich and A.T. Matthews, Paul Weidlinger, Consulting Engineer, Air Force Weapons Laboratory, Technical Report AFWL-TR-67-21, July 1967.

[6] "Spherically Symmetric Elastic-Plastic Shock Propagation", by M.B. Friedman, H.H. Bleich and R. Parnes, Proceedings, A.S.C.E., Vol. 91, No. EM 3, June 1965.

[7] "Stresses in an Elastic-Plastic Half-Space Due to a Superseismic Step Load", by A.T. Matthews and H.H. Bleich, Paul Weidlinger, Consulting Engineer, Ballistics Research Laboratory, Aberdeen Proving Ground, Technical Report No. 4, March 1966.

[8] "Exponentially Decaying Pressure Pulse Moving with Superseismic Velocity on the Surface of an Elastic-Plastic Half-Space", by H.H. Bleich and A.T. Matthews, Paul Weidlinger, Consulting Engineer, Forthcoming Technical Report for the Air Force Weapons Laboratory, February 1968.

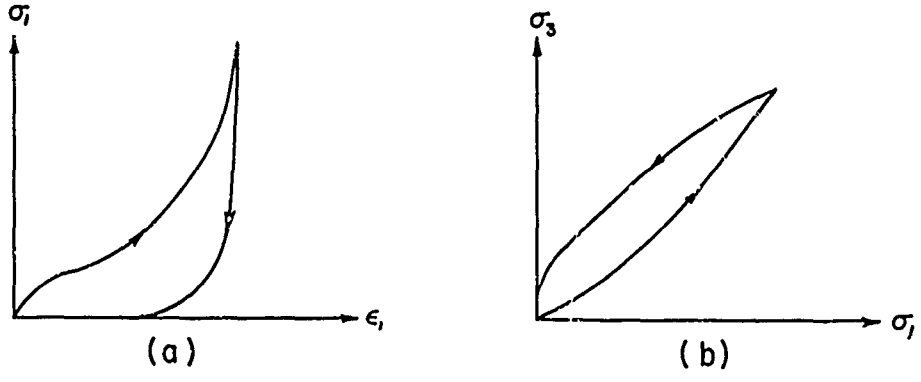

UNIAXIAL STRAIN

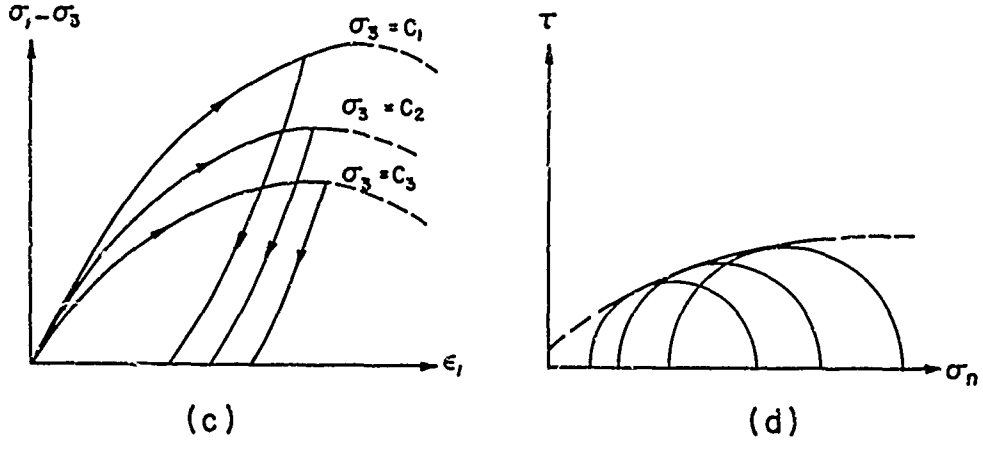

TRIAXIAL COMPRESSION

FIG. 1 TYPICAL EXPERIMENTAL RESULTS

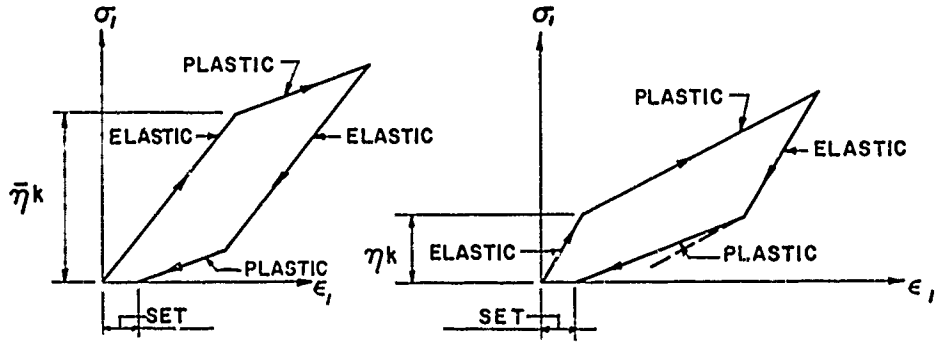

von MISES ELASTIC-PLASTIC
k LARGE

COULOMB - STRESS SMALL

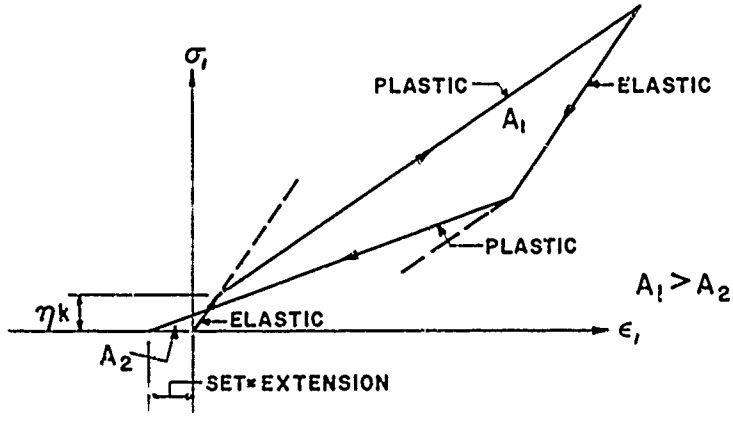

COULOMB - STRESS LARGE

FIG. 2 UNIAXIAL STRAIN — COULOMB AND von MISES MODELS
(CONSTANT BULK AND SHEAR MODULI)

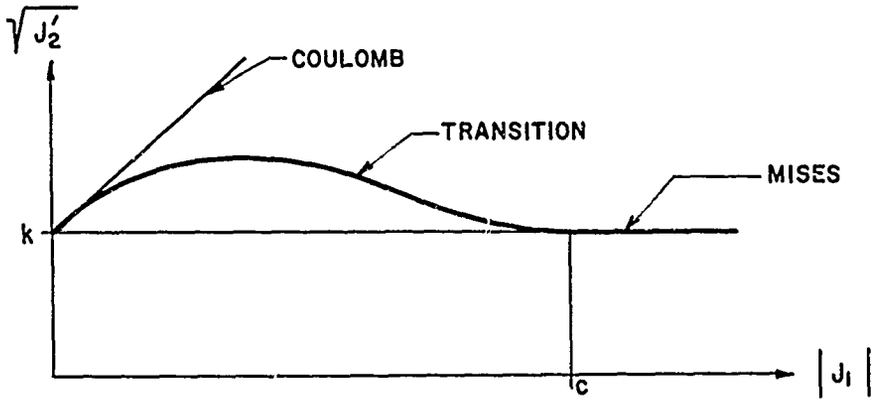

FIG. 3 YIELD CONDITION – TUFF MODEL

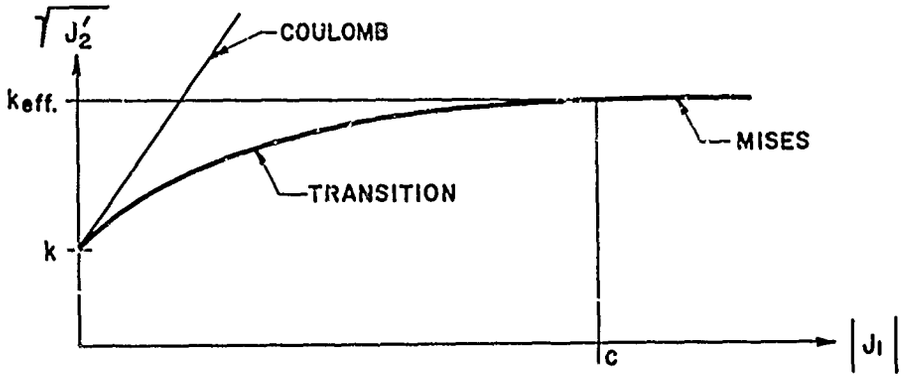

FIG. 4 YIELD CONDITION – ALLUVIUM – PLAYA MODEL

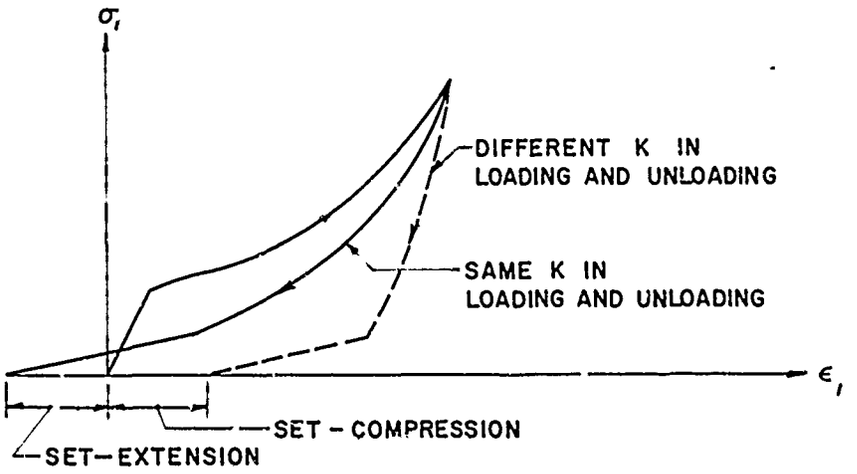

FIG. 5 UNIAXIAL STRAIN - ELIMINATION OF NET DILATION

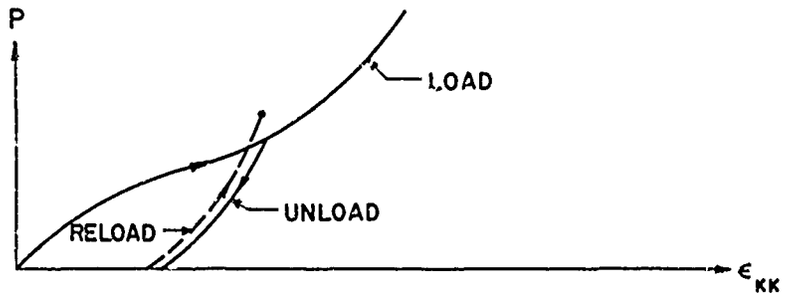

FIG. 6 — LOAD - UNLOAD — RELOAD RELATIONS
IN MATERIAL WHICH SUSTAINS DILATANCY

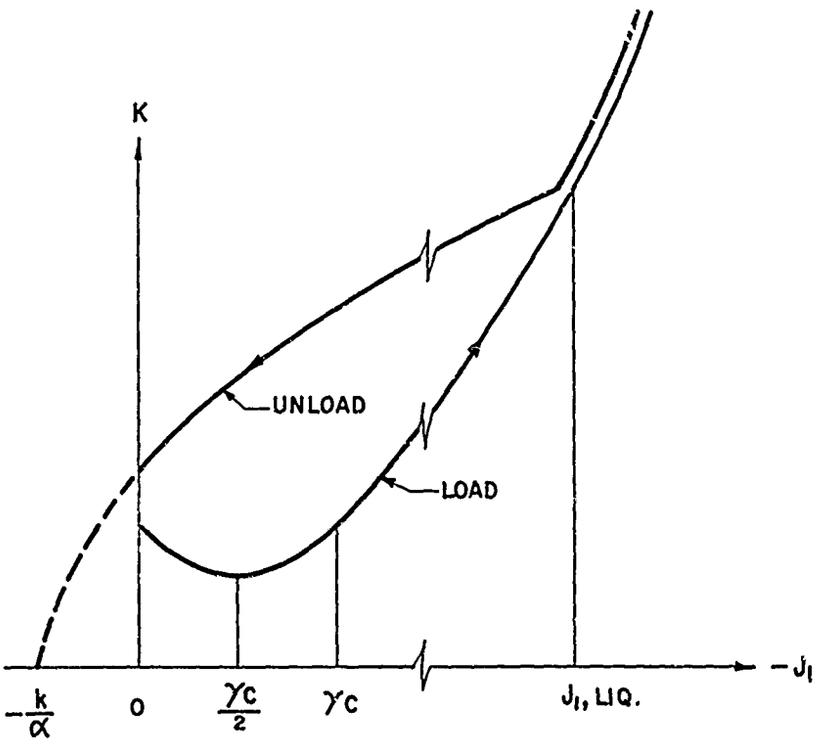

FIG. 7 NONLINEAR BULK MODULUS
LOADING AND UNLOADING
ALLUVIUM – PLAYA MATERIAL

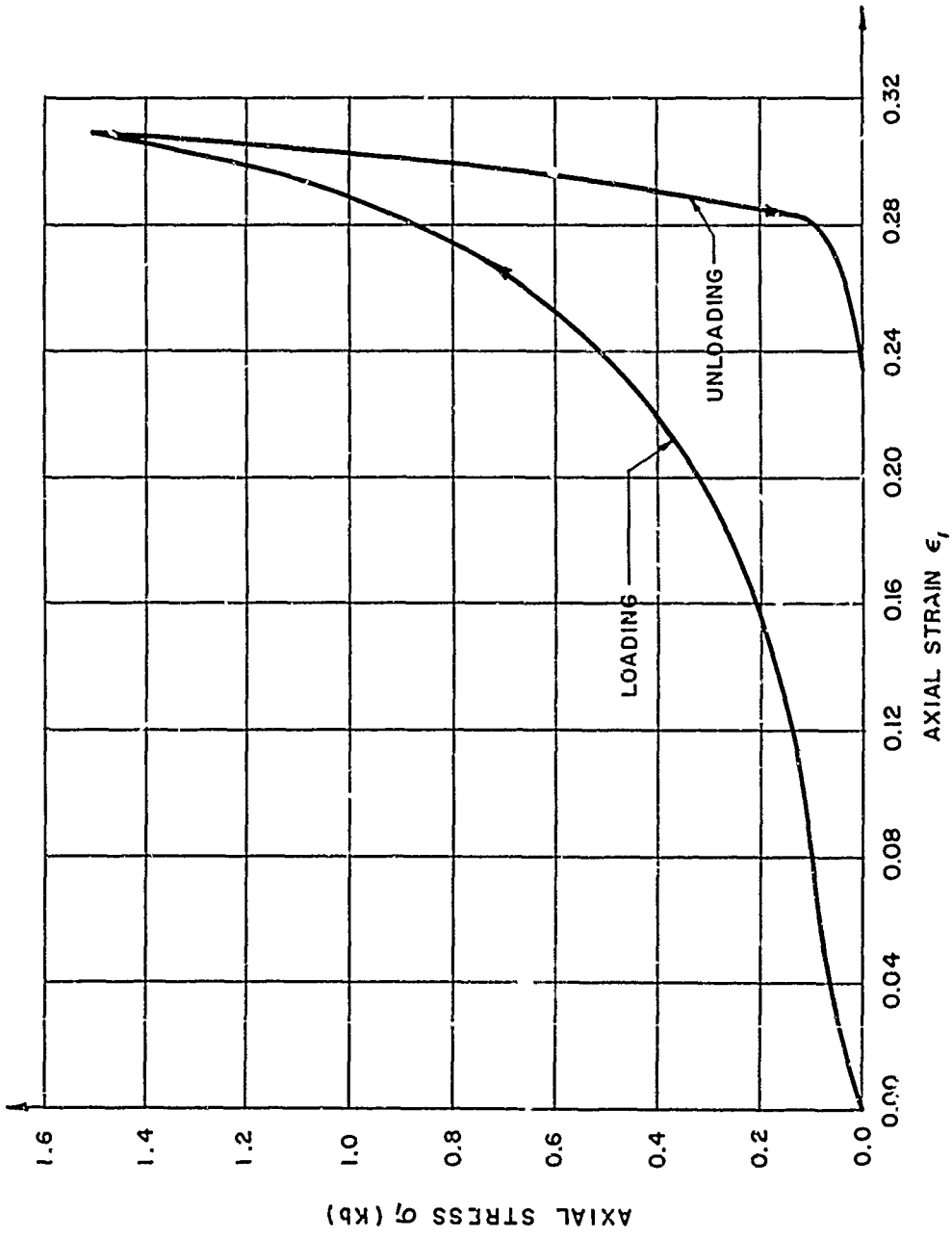

FIG. 8 STRESS – STRAIN RELATION IN UNIAXIAL STRAIN
ALLUVIUM – PLAYA MODEL

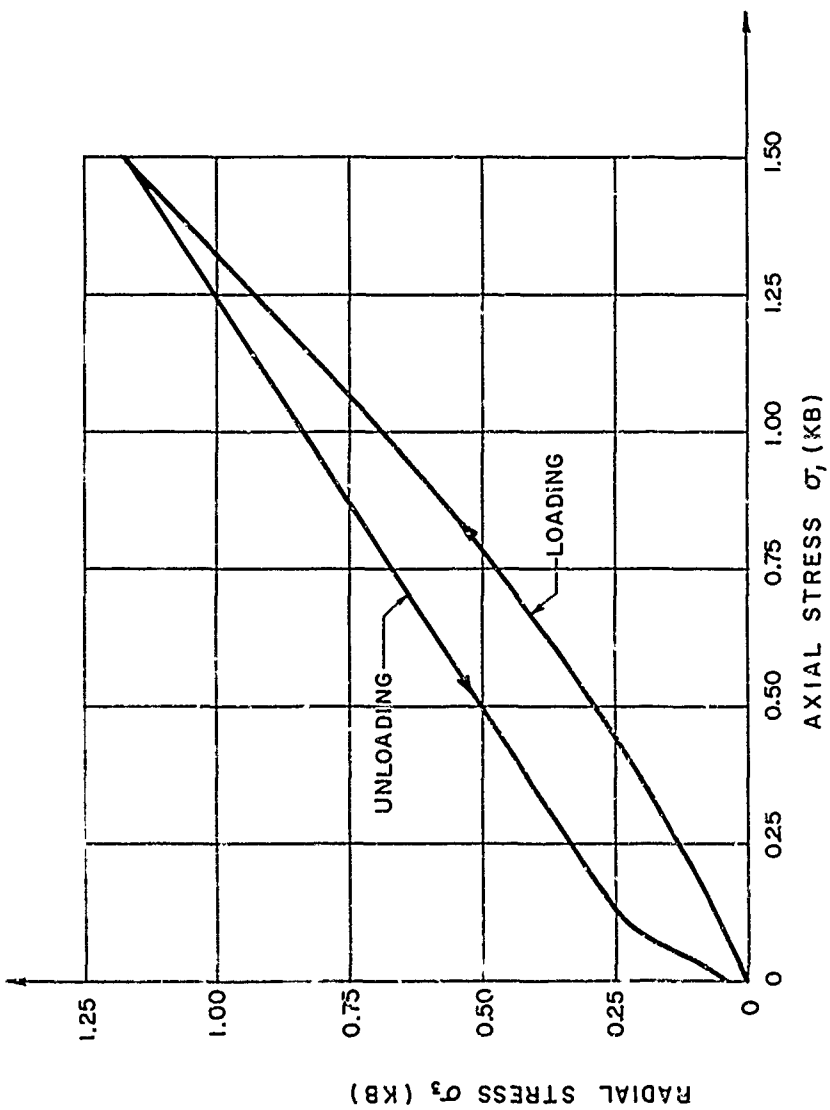

FIG. 9 RADIAL STRESS VS. AXIAL STRESS
LOADING AND UNLOADING IN UNIAXIAL STRAIN
ALLUVIUM -- PLAYA MODEL

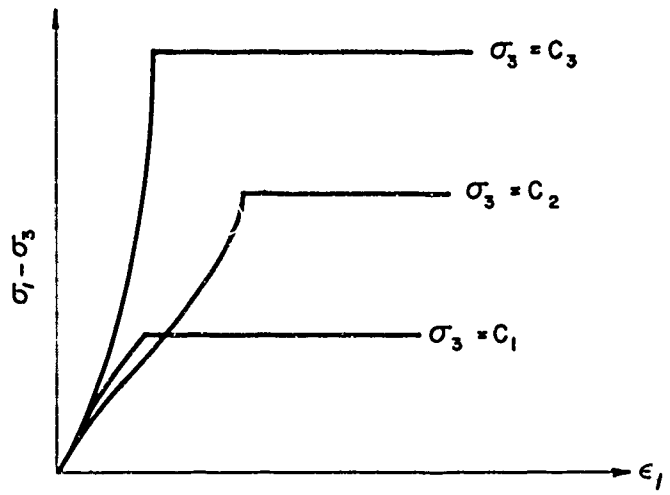

FIG. 10 TRIAXIAL COMPRESSION TEST
ALLUVIUM — PLAYA MODEL

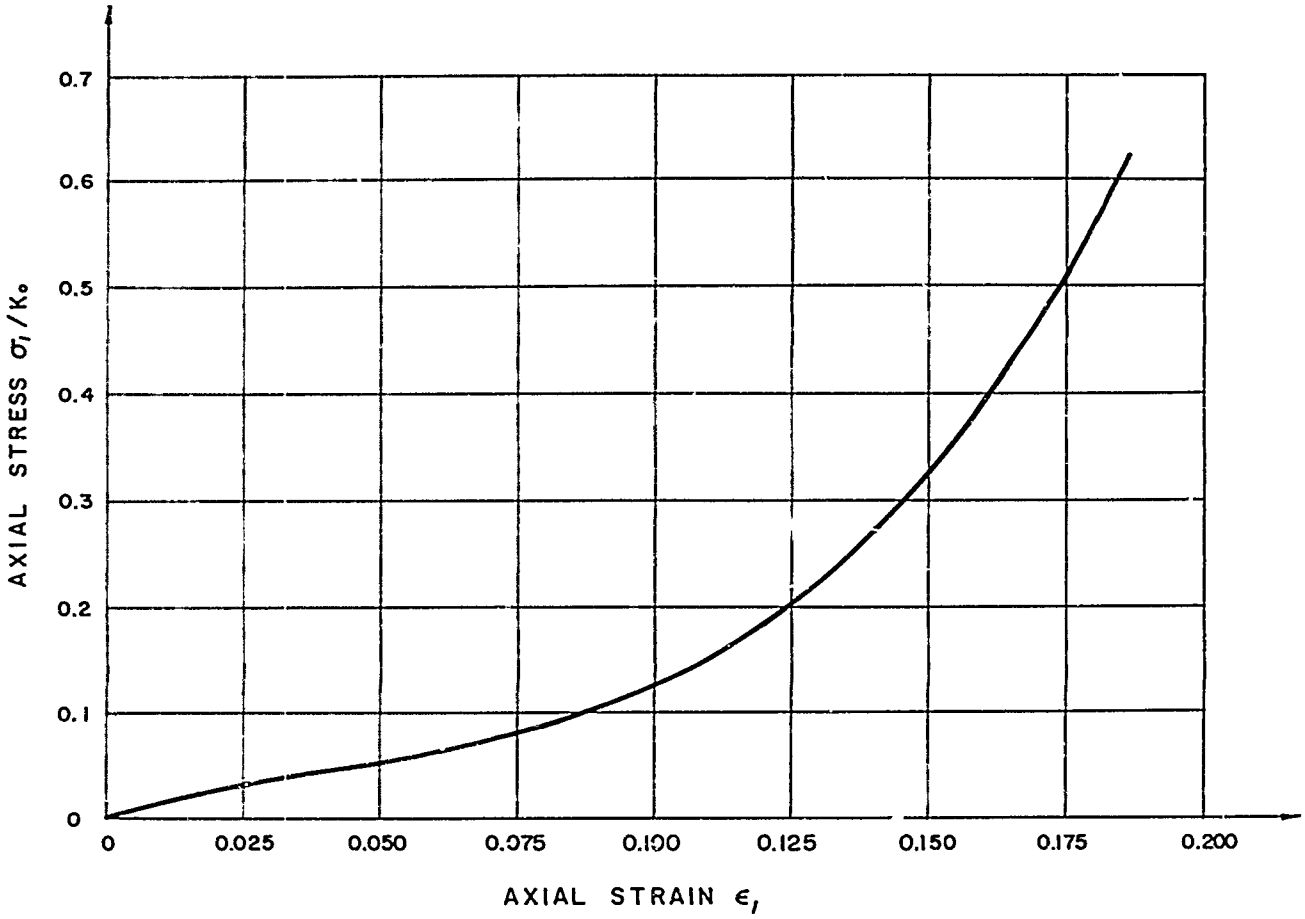

FIG. II STRESS—STRAIN RELATION IN UNIAXIAL STRAIN
VARIABLE MODULI MATERIAL, $K = K_o + K_1 e + K_2 e^2$; $G = G_o + G_1 e + \bar{G}_1 \sqrt{I_2'}$
(DRAWN FOR $\nu_o = 0.30$, $K_1/K_o = -100$, $K_2/K_o = 4000$, $G_1/K_o = 48$, $\bar{G}_1/K_o = -32$)

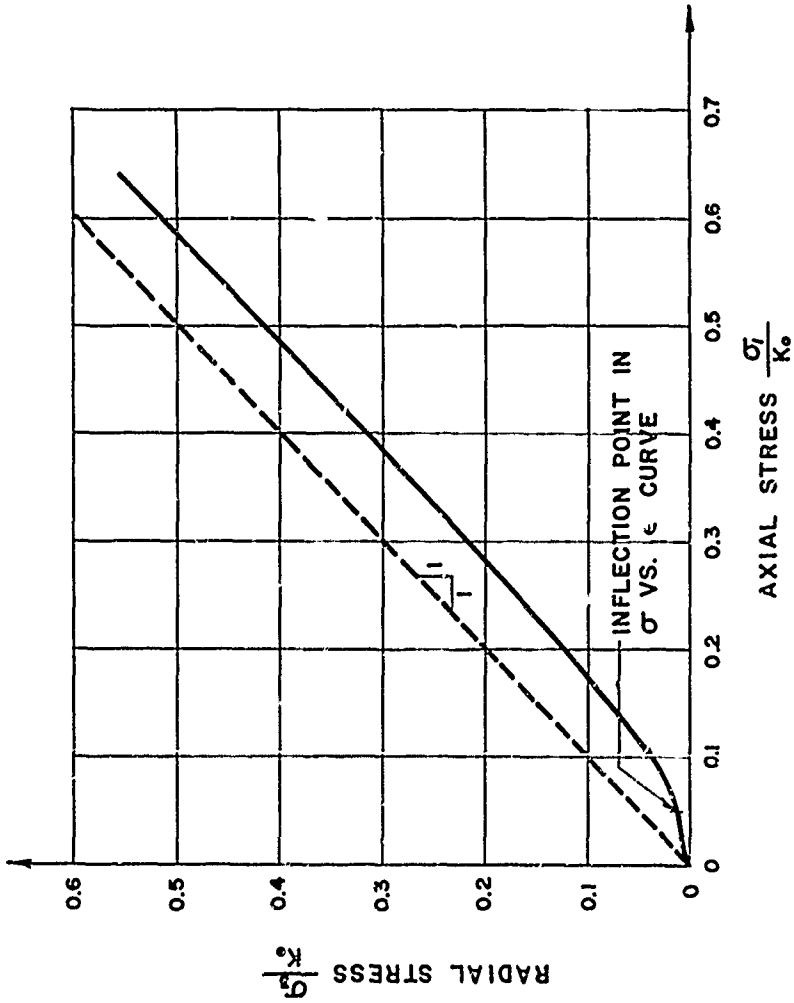

FIG. 12 RADIAL STRESS VS. AXIAL STRESS IN UNIAXIAL STRAIN VARIABLE MODULI MATERIAL, $K = K_o + K_1 e + K_2 e^2$; $G = G_o + G_1 e + \bar{G}_1 \sqrt{I_2'}$
(DRAWN FOR $\nu_o = 0.30$, $K_1/K_o = -100$, $K_2/K_o = 4000$, $G_1/K_o = 48$, $\bar{G}_1/K_o = -32$)

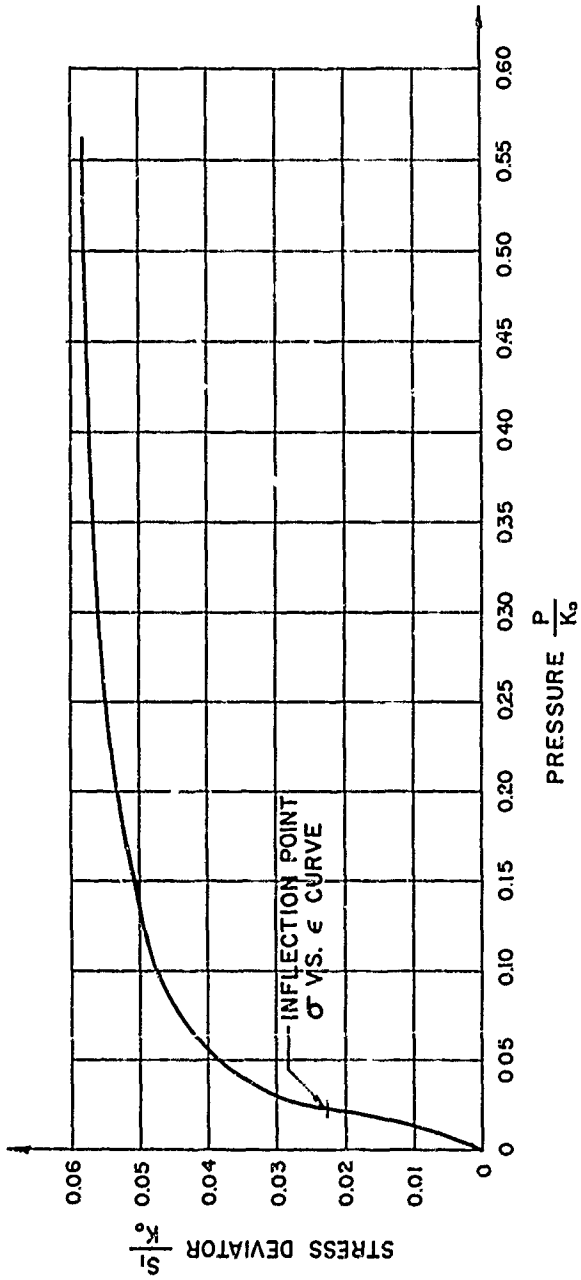

FIG.13 STRESS DEVIATOR VS. PRESSURE IN UNIAXIAL STRAIN
VARIABLE MODULI MATERIAL, $K = K_o + K_1 e + K_2 e^2$; $G = G_o + G_1 e + \bar{G}_1 \sqrt{I_2'}$
(DRAWN FOR $\nu_o = 0.30$, $K_1/K_o = -100$, $K_2/K_o = 4000$, $G_1/K_o = 48$, $\bar{G}_1/K_o = -32$)

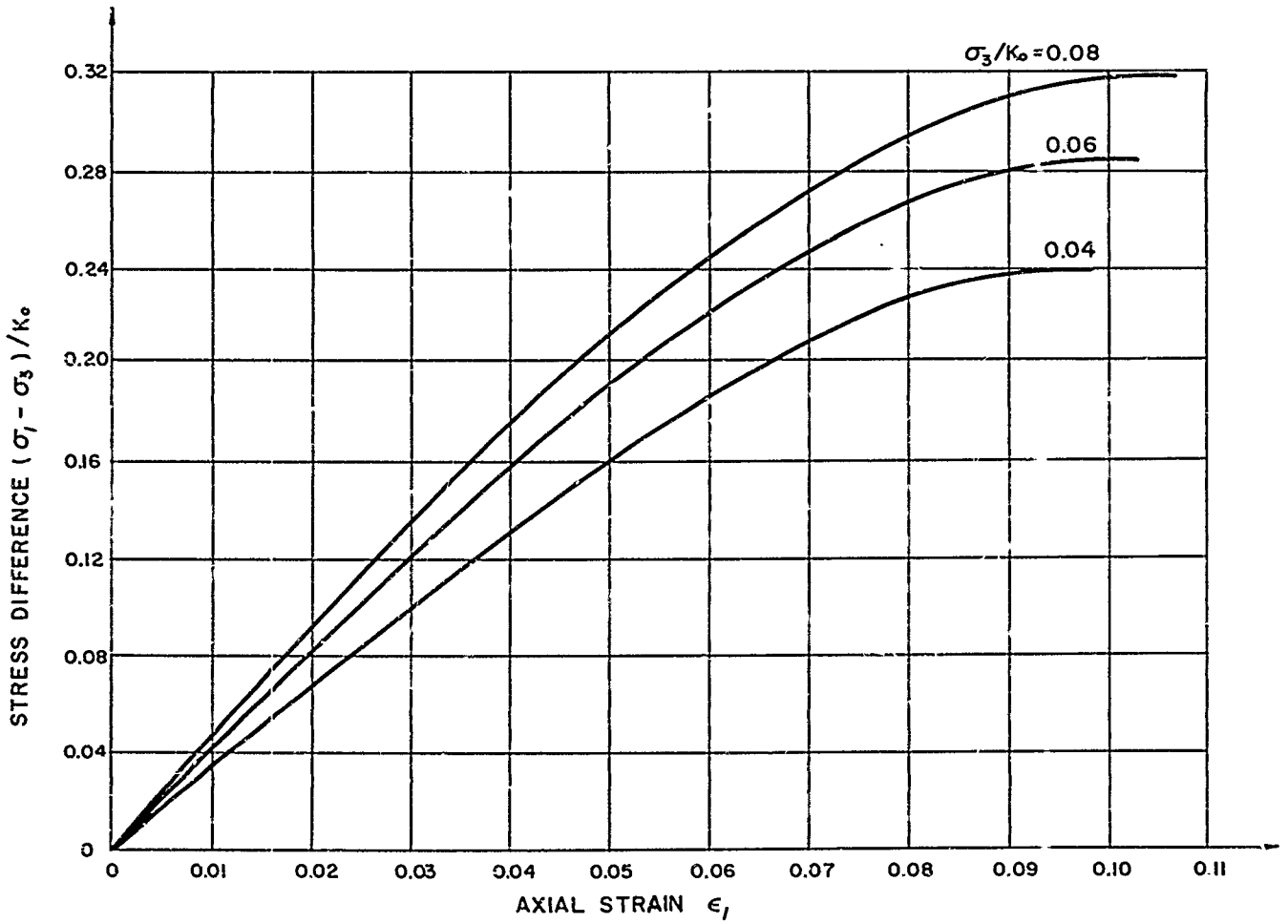

FIG. 14. TRIAXIAL COMPRESSION TEST

VARIABLE MODULI MATERIAL, $K = K_o + K_1 e + K_2 e^2$; $G = G_o + G_1 e + \bar{G}_1 \sqrt{I_2'}$

(DRAWN FOR $\nu_o = 0.30$, $K_1/K_o = -100$, $K_2/K_o = 4000$, $G_1/K_o = 48$, $\bar{G}_1/K_o = -32$)

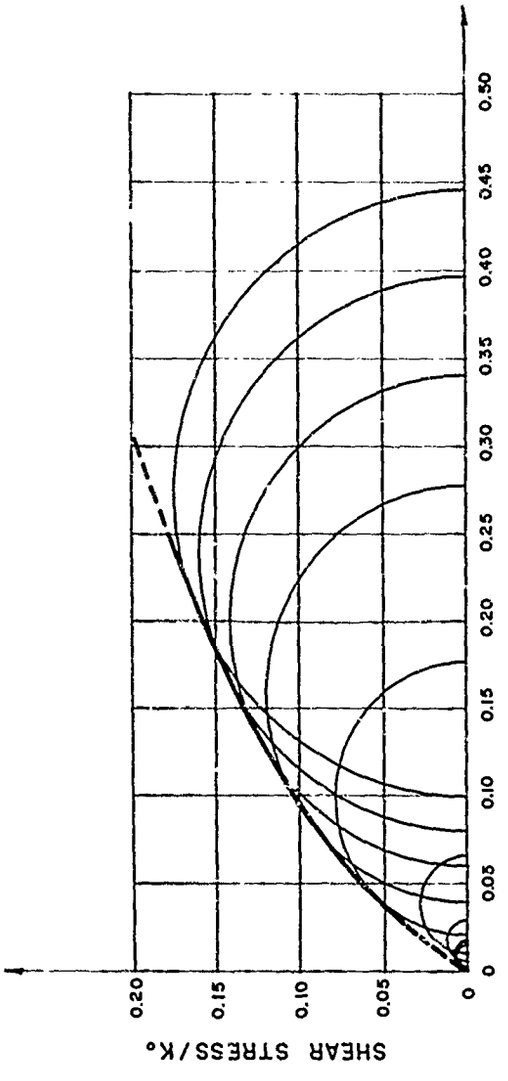

FIG. 15 MOHR ENVELOPE

VARIABLE MODULI MATERIAL, $K = K_0 + K_1 e + K_2 e^2$; $G = G_0 + G_1 e + \bar{G}_1 \sqrt{I_2'}$

(DRAWN FOR $\nu_0 = 0.30$, $K_1/K_0 = -100$, $K_2/K_0 = 4000$, $G_1/K_0 = 48$, $\bar{G}_1/K_0 = -32$)

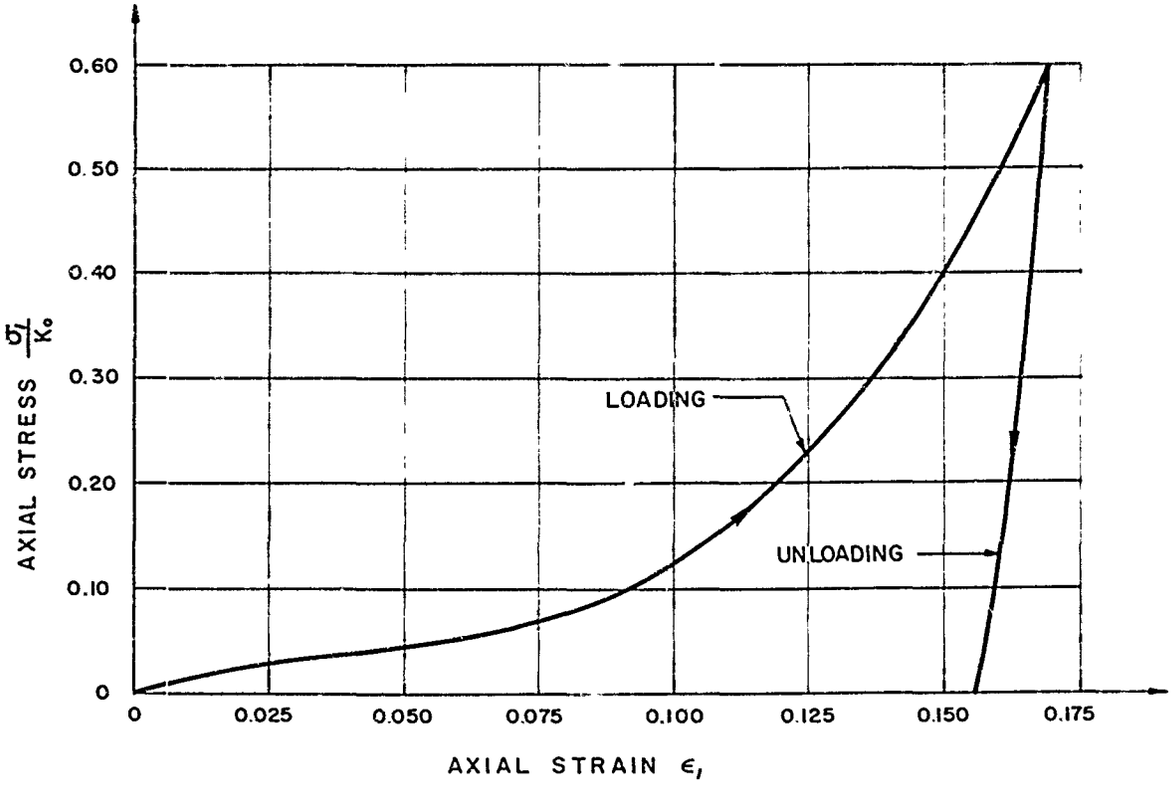

FIG. 16 STRESS – STRAIN RELATION IN UNIAXIAL STRAIN
VARIABLE MODULI MIXED MODEL, $K = K_o + K_1 e + K_2 e^2$; $G = G_o + \gamma_1 p + \overline{\gamma}_1 \sqrt{J_2'}$
(DRAWN FOR $\nu_o = 0.30$, $K_1/K_o = -100$, $K_2/K_o = 4000$, $\gamma_1 = 60$, $\overline{\gamma}_1 = -133.3$, $K_{UN}/K_o = 30$)

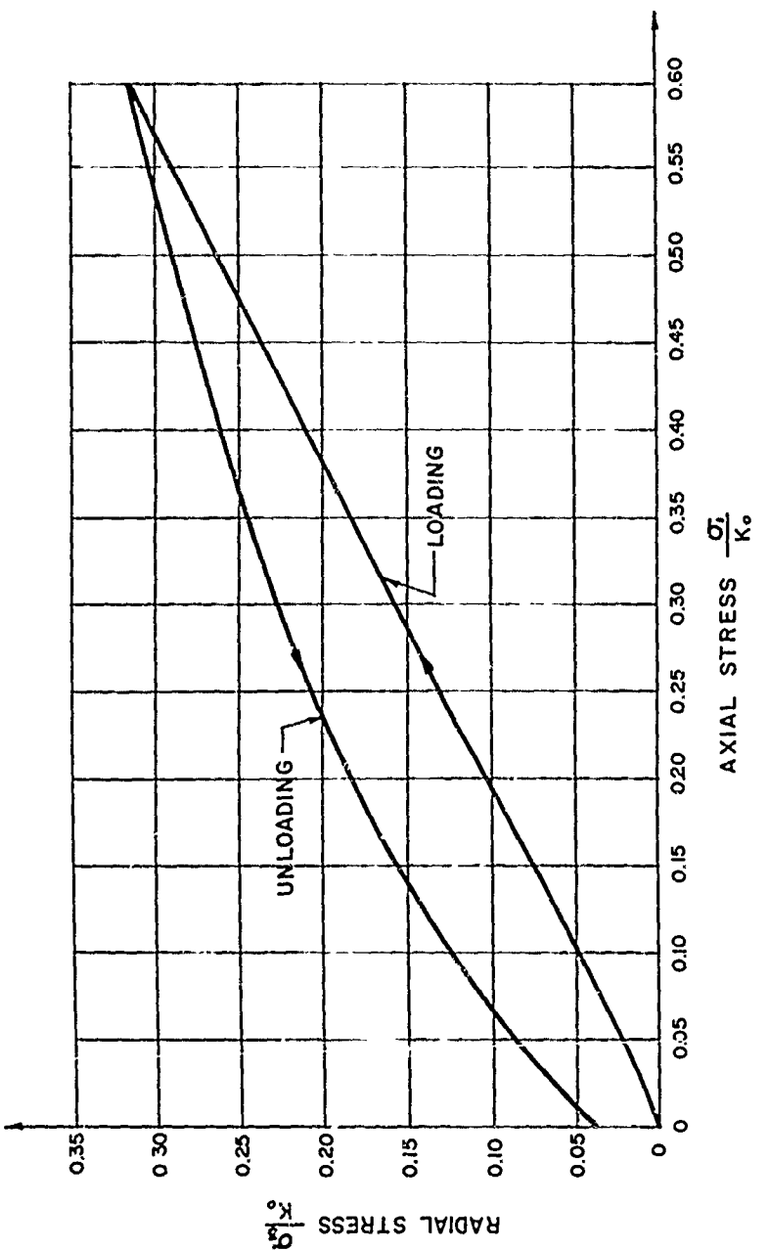

FIG. 17 RADIAL STRESS VS. AXIAL STRESS IN UNIAXIAL STRAIN
VARIABLE MODULI MIXED MODEL, $K = K_o + K_1 e + K_2 e^2$; $G = G_o + \gamma_1 \rho + \overline{\gamma}_1 \sqrt{J_2'}$
(DRAWN FOR $\nu_o = 0.30$, $K_1/K_o = -100$, $K_2/K_o = 4000$, $\gamma_1 = 60$, $\overline{\gamma}_1 = -133.3$, $K_{UR}/K_o = 30$)

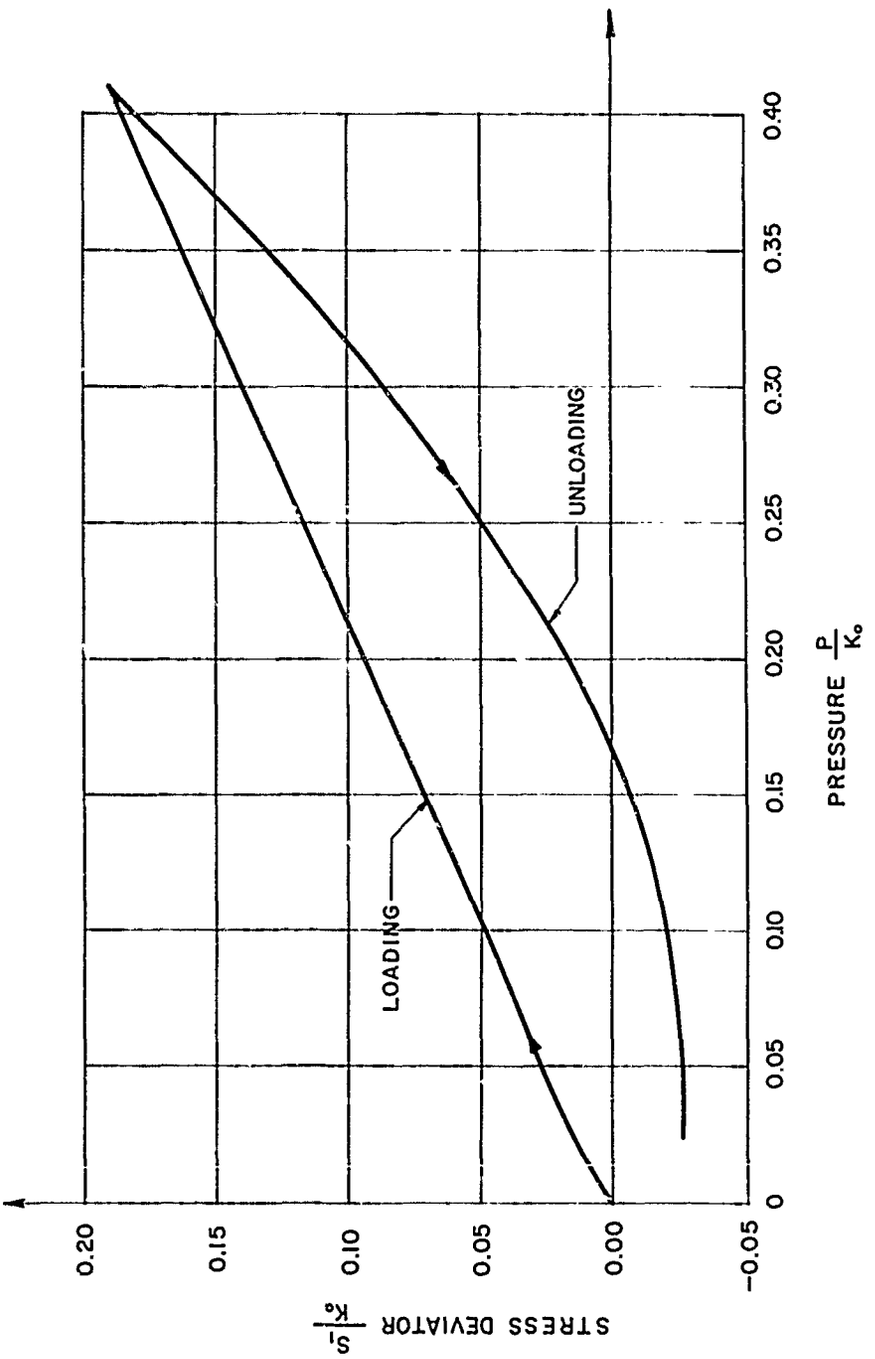

FIG. 18 STRESS DEVIATOR VS. PRESSURE IN UNIAXIAL STRAIN
VARIABLE MODULI MIXED MODEL, $K=K_o+K_1e+K_2e^2$; $G=G_o+\gamma_1 p+\overline{\gamma}_1\sqrt{J_2'}$
(DRAWN FOR $\nu_o=0.30$, $K_1/K_o=-100$, $K_2/K_o=4000$, $\gamma_1=60$, $\overline{\gamma}_1=-133.3$, $K_{UN}/K_o=30$)

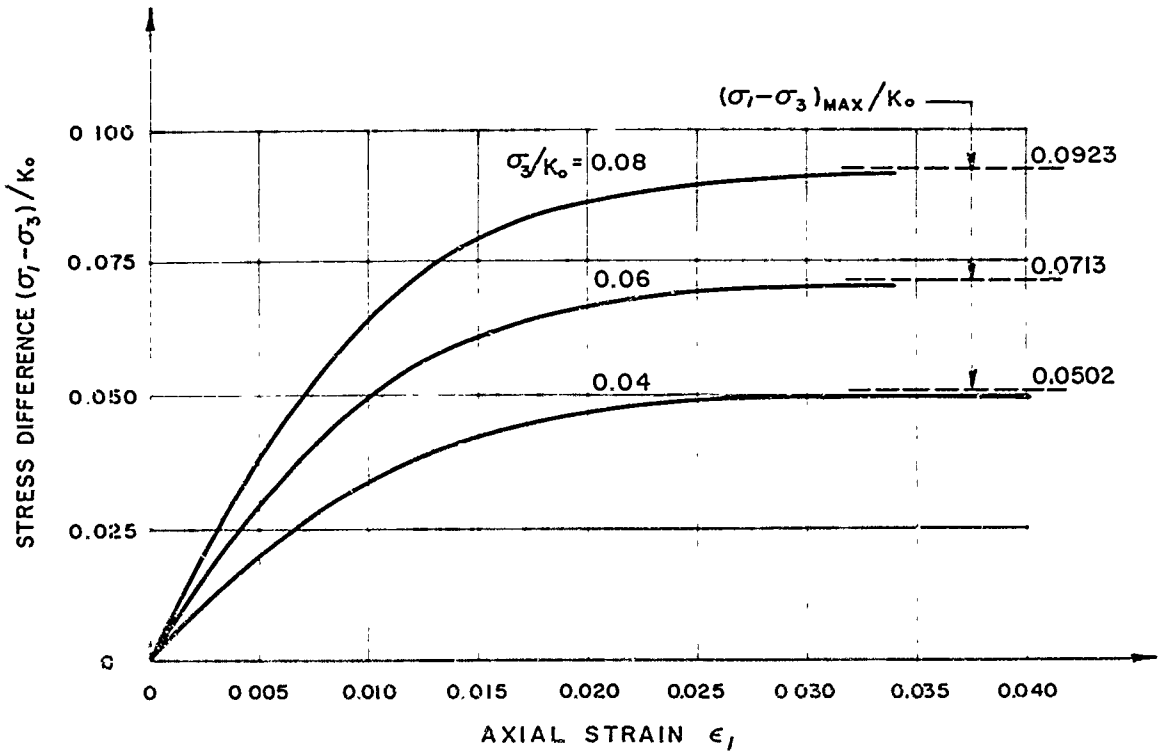

FIG. 19 – TRIAXIAL COMPRESSION TEST
VARIABLE MODULI MIXED MODEL, $K = K_o + K_1 e + K_2 e^2$; $G = G_o + \gamma_1 p + \bar{\gamma}_1 \sqrt{J_2'}$
(DRAWN FOR $\nu_o = 0.30$, $K_1/K_o = -100$, $K_2/K_o = 4000$, $\gamma_1 = 60$, $\bar{\gamma}_1 = -133.3$)

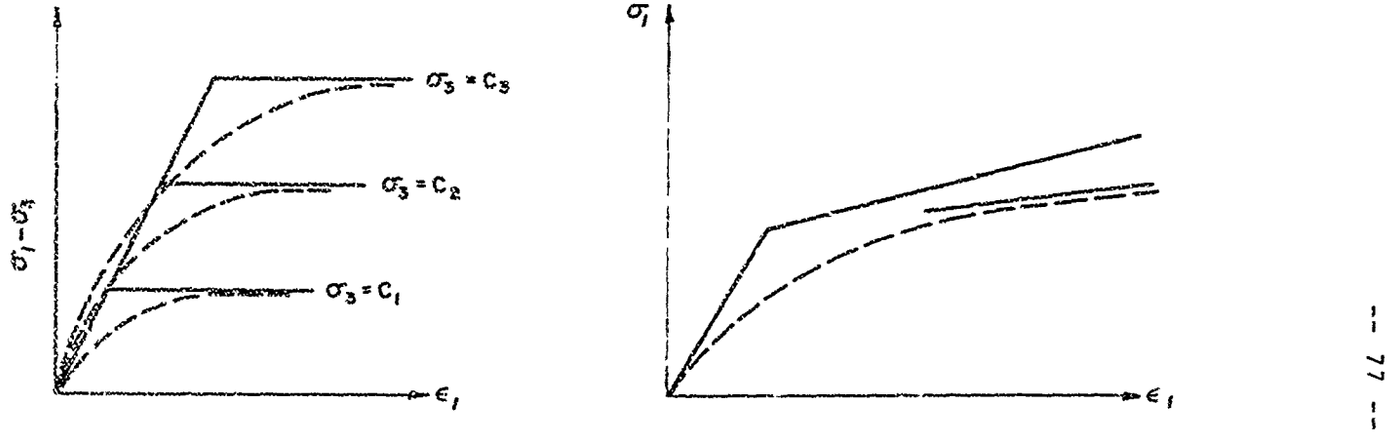

TRIAXIAL COMPRESSION TEST

UNIAXIAL STRAIN TEST

SOLID LINE – PRAGER – DRUCKER MATERIAL (CONSTANT K AND G)
DASHED LINE – COMBINED STRESS-STRAIN VARIABLE MODULI MODEL WITH $K_1 = K_2 = 0$

FIG. 20 COMPARISON OF VARIABLE MODULI AND PLASTIC MODELS

Unclassified

Security Classification

DOCUMENT CONTROL DATA - R & D

(Security classification of title, body of abstract and indexing annotation must be entered when the overall report is classified)

1 ORIGINATING ACTIVITY (Corporate author) Paul Weidlinger, Consulting Engineer New York, N. Y.	2a. REPORT SECURITY CLASSIFICATION Unclassified 2b. GROUP

3 REPORT TITLE

INVESTIGATION OF GROUND SHOCK EFFECTS IN NONLINEAR HYSTERETIC MEDIA: Report 1, DEVELOPMENT OF MATHEMATICAL MATERIAL MODELS

4 DESCRIPTIVE NOTES (Type of report and inclusive dates)
Report 1 of a series

5 AUTHOR(S) (First name, middle initial, last name)

Ivan Nelson
Melvin L. Baron

6 REPORT DATE	7a. TOTAL NO. OF PAGES	7b. NO OF REFS
March 1968	83	8

8a. CONTRACT OR GRANT NO.	9a. ORIGINATOR'S REPORT NUMBER(S)
DACA39-67-C-0048 b. PROJECT NO.	
c. d.	9b. OTHER REPORT NO(S) (Any other numbers that may be assigned this report) Contract Report S-68-1

10. DISTRIBUTION STATEMENT

This document has been approved for public release and sale; its distribution is unlimited.

11. SUPPLEMENTARY NOTES	12. SPONSORING MILITARY ACTIVITY
Prepared under contract for U. S. Army Engineer Waterways Experiment Station, Vicksburg, Mississippi	Defense Atomic Support Agency Washington, D. C.

13. ABSTRACT

A historical outline of mathematical models used previously to represent soil and rock behavior in ground shock computations at low pressure levels is presented. The problems and deficiencies of these early approaches are discussed. Subsequently, two types of models are developed; one a plastic model in which the yield condition depends on the mean stress and in which different variable bulk moduli are used in loading and unloading. The second type of model, called the "variable bulk moduli model," has variable shear as well as moduli, but no explicit yield condition. The behavior of both types of model in uniaxial strain and triaxial compression tests is examined.

DD FORM 1 NOV 68 1473 REPLACES DD FORM 1473, 1 JAN 64, WHICH IS OBSOLETE FOR ARMY USE.

Unclassified

Security Classification

Unclassified

Security Classification

14 KEY WORDS	LINK A		LINK B		LINK C	
	ROLE	WT	ROLE	WT	ROLE	WT
Hysteretic material models						
Elastic-plastic material models						
Ground shock						
Soil and rock models						

Unclassified

Security Classification